nature communications

Article

https://doi.org/10.1038/s41467-025-59449-z

Suppressing an auxin efflux transporter enhances rice adaptation to temperate habitats

Received: 12 August 2024

Accepted: 23 April 2025

Published online: 02 May 2025

Check for updates

Yanchun Cui[1,8], Lifang Huang[1,8], Peng Liu[1,8], Xiaodong Wang[1,2,8], Bi Wu[3], Yongjun Tan[4], Xuan Huang[1,2], Xiaojie Hu[1,5], Zhankun He[1], Yuqi Xia[1,2], Zebang Li[1,2], Wenli Zhang[6], Wenbang Tang[4], Yongzhong Xing[3], Caiyan Chen[1,2] & Donghai Mao[1,2,7]

Rice (*Oryza sativa* L.), a chilling-sensitive staple crop originating from tropical and subtropical Asia, can be cultivated in temperate regions through the introduction of chilling tolerance traits. However, the molecular mechanisms underlying this adaptation remain largely unknown. Herein, we show that *HAN2*, a quantitative trait locus, confers chilling tolerance in *temperate japonica* rice. *HAN2* encodes an auxin efflux transporter (OsABCB5) and negatively regulates chilling tolerance, potentially via auxin-mediated signaling pathway. During rice domestication, *HAN2* has undergone selective divergence between the *indica* and *temperate japonica* subspecies. In *temperate japonica* rice, the insertion of a *Copia* long terminal repeat retrotransposon downstream of *HAN2* reduces its expression, thereby enhancing chilling tolerance and facilitating adaptation to temperate climates. Introgression of the *temperate japonica HAN2* allele into *indica* rice significantly improves chilling tolerance at both seedling and booting stages. These findings advance our understanding of rice northward expansion and provide a valuable genetic resource for improving yield stability under chilling stress.

Chilling stress is a critical environmental stress factor that restricts crop growth and geographical distribution, thereby impacting crop yield. Rice, a staple food for over 50% of the global population, originated in tropical and subtropical regions and is inherently sensitivity to chilling stress[1]. Some rice ecotypes, such as whole *indica* rice and part of *tropical japonica* rice, which predominantly grow in tropical and subtropical areas, are particularly sensitive to chilling[1]. Conversely, *temperate japonica* rice acquired chilling tolerance and adapted to temperate regions during domestication[1]. Chilling tolerance in rice is a complex trait governed by quantitative trait loci (QTL). To date, many QTLs associated with the difference in chilling tolerance between *indica* and *japonica* rice have been primarily mapped across 12 rice chromosomes through linkage mapping or genome-wide association studies[2]. However, only a few of these QTLs have been identified and characterized, including *LTG1*[3], *COLD1*[4], *qCTS-9*[5], *LGS1*[6], *qCT7*[7], *HAN1*[1], *COLD11*[8], *COG1-4*[9–12], and *COLD6*[13] for seedling tolerance; *CTB1*[14], *CTB4a*[15], *bZIP73*[16], *CTB3*[17], *CTB5*[18], and *CTB6*[19] for booting tolerance; *qLTG3-1*[20] and *OsUBC12*[21] for germination tolerance. To develop climate-resilient rice varieties, it is essential to clone more chilling tolerance QTLs from rice.

Plants have evolved various strategies to rapidly sense, respond and adapt to chilling stress via calcium signalling, MAPK cascades, and

[1]Institute of Subtropical Agriculture, Chinese Academy of Sciences, Changsha, China. [2]University of Chinese Academy of Sciences, Beijing, China. [3]Yazhou Bay National Laboratory, Sanya, China. [4]State Key Laboratory of Hybrid Rice, Hunan Hybrid Rice Research Center, Changsha, China. [5]UWA School of Agriculture and Environment, The University of Western Australia, Perth, Australia. [6]State Key Laboratory of Crop Genetics and Germplasm Enhancement and Utilization, CIC-MCP, Nanjing Agricultural University, Nanjing, China. [7]Yuelushan Laboratory, Changsha, China. [8]These authors contributed equally: Yanchun Cui, Lifang Huang, Peng Liu, and Xiaodong Wang. e-mail: donghai.mao@isa.ac.cn

transcription factors. The potential chilling sensors COLD1 trigger calcium (Ca^{2+}) signalling to confer chilling tolerance in cells, while a chilling sensor complex of COLD6 and osmotin-like 1 (OSM1) triggers 2′, 3′-cyclic adenosine monophosphate (2′, 3′-cAMP) production to enhance chilling tolerance in rice[4,13]. These chilling-induced second messenger signals can be sensed by MAPK cascades, which transduce the low-temperature signals downstream via phosphorylation pathways, thereby facilitating the adaptive responses to chilling stress. Among them, *OsMAP1*/*OsMAPK3* is a gene that encodes a mitogen-activated protein kinase and plays a crucial role in regulating chilling tolerance during both the seedling and flowering stages[22,23]. Calcium-dependent protein kinase can direct phosphorylate and activate *OsMAP1*/*OsMAPK3* to improve chilling tolerance in rice[24]. Chilling signals can also be transited by MAPK cascades, such as OsMKK6-OsMPK3, to enhance chilling tolerance in rice[25]. OsMAP1/OsMAPK3 phosphorylates and stabilises OsbHLH002, which targets *OsTPP1* to increase its transcription, leading to increased trehalose level and enhanced chilling tolerance in rice[22]. In addition to OsMAP1/OsMAPK3, chilling signalling is transited by many transcription factors, such as OsMADS57[26], OsTB1[26], OsWRKY94[26], MYBS3[27], OsGRF6[28], and OsWRKY76[29] to balance the tolerance and growth. However, it remains unreported whether the pivotal gene *OsMAP1*/*OsMAPK3*, which regulates chilling tolerance concurrently at the seedling and booting stages, is subject to regulation by transcription factors.

Plant hormones play a crucial role in regulating the chilling tolerance of rice. Hormones such as jasmonic acid (JA), abscisic acid (ABA), and ethylene are instrumental in enabling rice to adapt to chilling environments by modulating physiological and molecular mechanisms[30]. *HAN1* encodes a monooxygenase from the cytochrome P450 family that facilitates the conversion of active jasmonoyl-L-isoleucine to inactive 12-hydroxy-jasmonoyl-L-isoleucine. This process regulates JA-mediated responses to chilling stress and enhances chilling tolerance in rice[1]. $bZIP73^{Jap}$ interacts with bZIP71 to modulate ABA levels and maintain a balance of reactive oxygen species, consequently enhancing rice's resilience to chilling stress[16]. *OsUBC12* encodes an E2 ubiquitin-conjugating enzyme that negatively regulates ABA signalling[21]. Auxin plays a crucial role in plant growth, development, and environmental adaptation. A previous study reported the impact of auxin on the adaptability of plants to chilling stress[31]; however, the exact mechanism by which auxin regulates chilling tolerance is still not well understood. Moreover, no studies have reported on the involvement of auxin in the formation of chilling tolerance traits in *temperate japonica* rice during domestication.

In this study, we isolate and functionally characterize one of the QTL genes, which is named *HAN2* ("HAN" means "chilling" in Chinese). *HAN2* encodes an ABCB transporter (OsABCB5) with auxin efflux function. The gene negatively regulates chilling tolerance in rice, potentially via auxin-mediated signalling pathway. Introgression of the *temperate japonica* rice allele of *HAN2*, which contains a *Copia* long terminal repeat retrotransposon (*Copia* LTR) insertion downstream, not only enhances chilling tolerance at both seedling and booting stages but also demonstrates its potential for improving yield stability and supporting climate-resilient rice breeding.

Results

HAN2 negatively regulates chilling tolerance in rice

Temperate japonica rice typically exhibits stronger chilling tolerance than *indica* rice (Supplementary Fig. 1a-b). The genetic bases of chilling tolerance were investigated using a set of chromosome segment substitution lines derived from a backcross between the *temperate japonica* donor cultivar Nipponbare (NPB) and the *indica* recipient cultivar 93-11. The results showed that the chilling tolerance of NIL-$HAN2^{NPB}$ was approximately twice that of 93-11 (Fig. 1a, b). Genome-wide genotyping revealed a substituted segment spanning the 26.0–29.9 Mb interval on chromosome 1 (Supplementary Fig. 2). This suggests the presence of a QTL in this region, named *HAN2*, which confers chilling tolerance in rice, consistent with previously reported findings[32].

To isolate the causal QTL gene underlying *HAN2*, NIL-$HAN2^{NPB}$ was further backcrossed to 93-11 for high-resolution mapping, generating approximately 3200 BC_1F_2 progeny plants. Based on the chilling tolerance performance of seedlings among these progeny lines, *HAN2* was mapped to the interval flanked by markers M4 (R1ID2876) and M5 (R1ID2879) and further narrowed to a 30.0 kb genomic region containing three predicted genes (Fig. 1c, Supplementary Fig. 3a–f and Supplementary Table 1). Within this 30.0 kb interval, *LOC_Os01g50090* was identified as a retrotransposon. Differential expression analysis revealed that the auxin transporter gene *OsABCB5* (*LOC_Os01g50100*) was the only gene exhibiting significant differential expression in seedlings shoot between the two parental lines (Fig. 1d and Supplementary Fig. 4). Additionally, *LOC_Os01g50100* expression changed markedly in response to chilling stress (Supplementary Fig. 5a), and its expression level was significantly higher in *indica* rice than *temperate japonica* rice (Supplementary Fig. 5b). Based on these findings, we identified *OsABCB5* as the candidate gene for *HAN2*.

To validate whether *OsABCB5* is *HAN2*, knockout and overexpression lines were developed in the background of temperate *japonica* rice cultivar ZH11. In the CRISPR/Cas9-derived knockout lines *han2*-1 and *han2*-2, chilling tolerance was significantly enhanced at the seedling stage (Fig. 1e, f and Supplementary Fig. 6a), whereas chilling tolerance was reduced in the overexpression lines (Fig. 1g, h and Supplementary Fig. 6b). Introduction of the p*HAN2*::$HAN2^{93\text{-}11}$-*GUS* expression vector into NIL-$HAN2^{NPB}$ resulted in transgenic lines with elevated *HAN2* expression and decreased chilling tolerance (Supplementary Fig. 7a–c). These results confirm that *OsABCB5* corresponds to *HAN2*, which negatively regulates chilling tolerance in rice.

HAN2 functions as an auxin efflux transporter

HAN2 was predicted to encode the ABCB transporter OsABCB5, which may be involved in auxin transport (Supplementary Fig. 8a, b). To validate the role of HAN2/OsABCB5 in auxin transport, we conducted a series of transport activity assays. First, we performed a deuterium-labelled auxin 3-indoleacetic acid-d_5 (d_5-IAA) transport assay in yeast cells. No significant difference in d_5-IAA content was observed between *HAN2-GFP* and *GFP*-expressing yeast cells after 3 h of incubation with 150 μM d_5-IAA (Supplementary Fig. 9a, b). However, after 12 h of efflux, d_5-IAA content was significantly lower in *HAN2-GFP*-expressing cells than in the *GFP* controls (Fig. 2a, b). Second, in *Xenopus* oocytes, no significant difference in d_5-IAA content was observed between *GFP-HAN2* and *GFP*-expressing oocytes after 4 h of incubation with 150 μM d_5-IAA (Supplementary Fig. 9c). However, following 4 h of efflux, *GFP-HAN2*-expressing oocytes exhibited a more pronounced reduction in d_5-IAA levels compared with *GFP*-expressing oocytes (Fig. 2c, d). Additionally, a d_5-IAA transport activity assay in rice protoplasts showed that wild type (WT) protoplasts had a significantly higher relative transfer of d_5-IAA efflux than *han2* protoplasts at 1 h, and 2 h (Fig. 2e). These results demonstrate that HAN2 functions as an auxin efflux transporter.

The expression pattern of *HAN2* was examined to understand its functional role. RT-qPCR analysis showed that *HAN2* was primarily expressed in the leaf, with particularly high expression in mature leaf (Supplementary Fig. 10a, b). This result was further validated by GUS histochemical staining in p*HAN2*::$HAN2^{93\text{-}11}$-*GUS* transgenic lines (Supplementary Fig. 10c). Immunofluorescence analysis using an anti-GUS antibody in these transgenic lines revealed that HAN2 is localized in the vascular bundle sheath parenchyma cells of the leaf (Supplementary Fig. 10d). Additionally, subcellular localization assays demonstrated that HAN2 resides in the plasma membrane of rice protoplasts (Supplementary Fig. 10e). Together, these findings indicate that HAN2 functions as an auxin transporter in the xylem of mature leaves.

https://doi.org/10.1038/s41467-025-59449-z

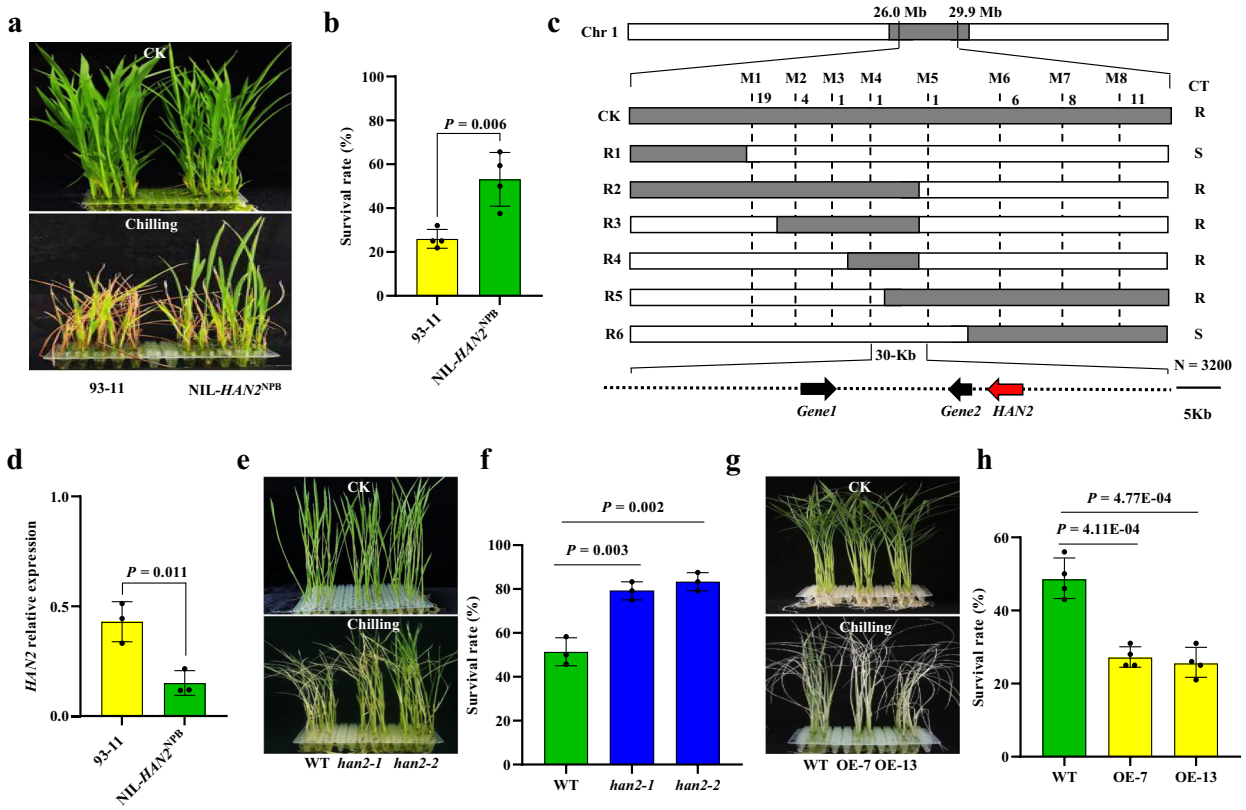

Fig. 1 | Map-based cloning of *HAN2*. **a** Chilling tolerance phenotype of 93-11 and NIL-*HAN2*^{NPB} plants. Seedlings were incubated at 10 °C for 5 days and then transferred to normal temperature for a 7 day recovery. Upper and lower panels show 93-11 and NIL-*HAN2*^{NPB} before and after chilling treatment, respectively. **b** Survival rates of 93-11 and NIL-*HAN2*^{NPB} after recovery. Data represent mean ± SD ($n = 4$ biological replicates, 16 seedlings per replicate). **c** Local genomic structure of key recombinants and performance of their progeny after chilling treatment. CT: chilling tolerance; T: tolerant; S: sensitive; grey bars represent heterozygous regions. **d** *HAN2* expression levels in 93-11 and NIL-*HAN2*^{NPB}. Data represent mean ± SD ($n = 3$ biological replicates, 3 seedlings per replicate). **e** Chilling tolerance phenotype of WT and *han2*. Seedlings were incubated at 4 °C for 5 days and recovered at normal temperature for 7 days. Upper and lower panels show WT and *han2* plants before and after treatment. **f** Survival rates of WT and *han2* plants after chilling treatment. Data represent mean ± SD ($n = 3$ biological replicates, 24 seedlings per replicate). **g** Chilling tolerance phenotype of WT and *HAN2*-overexpression lines. Seedlings were incubated at 10 °C for 5 days and recovered for 7 days. **h** Survival rates of WT and *HAN2*-overexpression lines after treatment. Data represent mean ± SD ($n = 4$ biological replicates, 16 seedlings per replicate). Statistical significance in (**b**–**h**) was evaluated using a two-tailed Student's *t*-test (*P*-values indicated). Source data are provided as a Source Data file.

Plants can synthesize auxin locally, including within leaves, through the highly conserved TAA/YUC pathway[33,34]. HAN2 may then transport the auxin synthesized in mature leaves to other tissues. This hypothesis was supported by results from leaf-feeding experiments using d_5-IAA, which showed that the relative transfer rate of d_5-IAA was significantly higher in WT plants than in *han2-2* mutants (Fig. 2f, g). Auxin quantification further revealed that auxin content in the young leaves of NIL-*HAN2*^{NPB} was significantly lower than that in 93-11(Fig. 2h). and similarly, *han2* mutants had significantly lower auxin content in young leaves compared with WT (Fig. 2i). An analysis of whole-plant auxin levels showed that NIL-*HAN2*^{NPB}, which has reduced *HAN2* expression both before and after chilling treatment, exhibited significantly lower auxin content than 93-11 (Supplementary Fig. 11a). Similarly, *han2*-2 mutants displayed notably lower auxin levels than WT plants (Supplementary Fig. 11b), whereas overexpression lines showed increased auxin accumulation (Supplementary Fig. 11c). These findings indicate that HAN2/OsABCB5 not only facilitates the transport of auxin from mature leaves to young leaves but also influences overall auxin levels throughout the plant.

HAN2 regulates chilling tolerance potentially via auxin-mediated signalling pathway

Auxin promotes the polyubiquitination and subsequent degradation of Aux/IAA proteins via the 26S proteasome, thereby releasing auxin response factors (ARFs) to activate or repress the expression of downstream responsive genes[35]. To determine whether *HAN2* regulates chilling tolerance through auxin signal transduction, chilling tolerance was assessed in different *HAN2* genotypes following exogenous auxin application. In the absence of exogenous auxin, NIL-*HAN2*^{NPB} exhibited a significantly higher survival rate than 93-11, and *han2* mutants showed significantly greater survival than WT plants. However, in the presence of exogenous auxin, the differences in chilling tolerance between NIL-*HAN2*^{NPB} and 93-11 as well as between *han2* and WT were reduced (Fig. 3a–d). Previous auxin measurements confirmed that NIL-*HAN2*^{NPB} and *han2* plants had significantly lower auxin levels compared with 93-11 and WT, respectively (Supplementary Fig. 11a, b). *HAN2* was also found to regulate the expression of *OsYUC8* (Supplementary Fig. 12a–d), which influences local auxin biosynthesis. Notably, auxin content was significantly lower in *osyuc8* mutants than in WT plants, and this reduction was associated with enhanced chilling tolerance (Supplementary Fig. 13a–e). Together, these findings demonstrate that *HAN2* negatively regulates chilling tolerance in rice through modulation of auxin signalling.

To investigate how *HAN2* regulates chilling tolerance in rice, the key chilling tolerance gene *OsMAP1*/*OsMPK3*[22–25] was identified among the differentially expressed genes in chilling stress transcriptomes (Supplementary Fig. 14a–e). Compared to their respective controls, 93-11 or WT, *OsMAP1*/*OsMPK3* was significantly upregulated in

https://doi.org/10.1038/s41467-025-59449-z

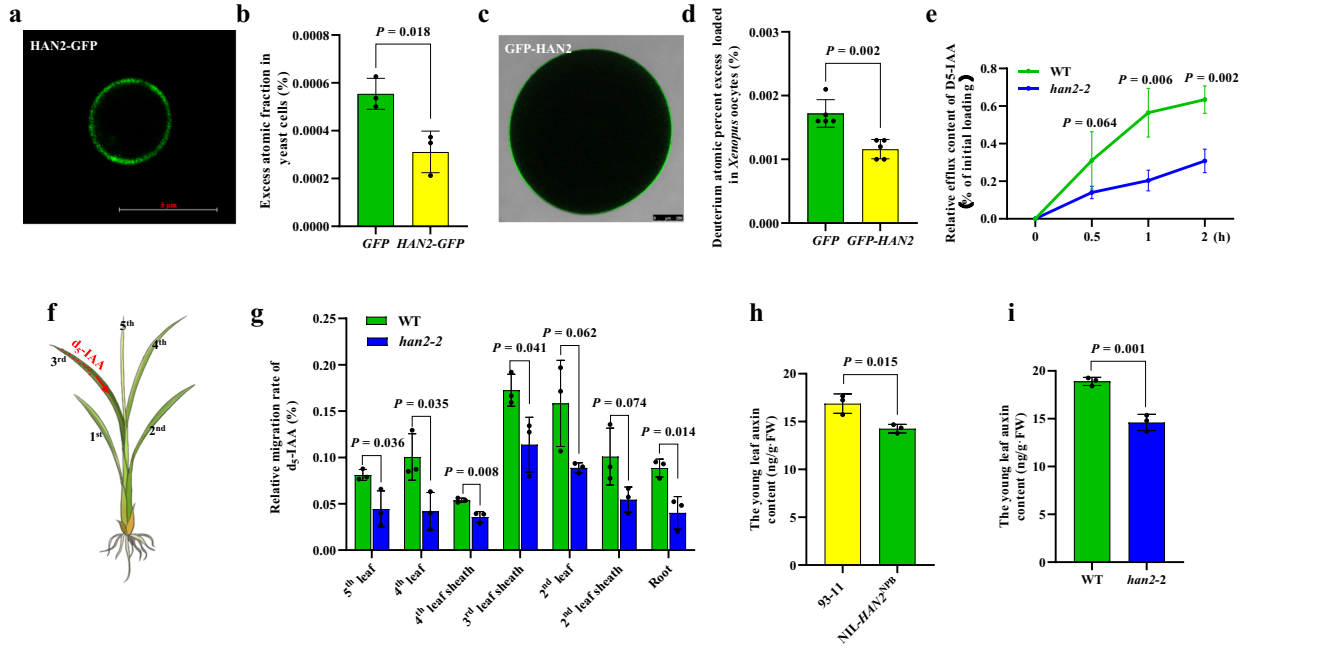

Fig. 2 | Functional analysis of HAN2 in auxin efflux transport. a Subcellular localisation of HAN2-GFP in *Saccharomyces cerevisiae* (yeast). Bar = 5 μm. **b** d_5-IAA efflux activity in yeast cells expressing HAN2-GFP. Data are shown as mean ± SD (n = 3 biological replicates). **c** Subcellular localisation of GFP-HAN2 in *Xenopus* oocytes. Bar = 50 μm. **d** d_5-IAA efflux activity in *Xenopus* oocytes expressing GFP-HAN2. Data are shown as mean ± SD (n = 5 biological replicates, with 3 oocytes per replicate). **e** d_5-IAA efflux activity in protoplasts of WT and *han2-2* mutants over different time periods. Data are shown as mean ± SD (n = 3 biological replicates). **f** Schematic diagram of the d_5-IAA feeding experiment from the third leaf. **g** Relative d_5-IAA transfer efficiency in WT and *han2-2* mutants. Data are shown as mean ± SD (n = 3 biological replicates, with 3 seedlings per replicate). **h** Auxin content in young leaves of 93-11 and NIL-*HAN2*^{NPB} seedlings. Data are shown as mean ± SD (n = 3 biological replicates, with 10 seedlings per replicate). **i** Auxin content in young leaves of WT and *han2-2* seedlings. Data are shown as mean ± SD (n = 3 biological replicates, with 10 seedlings per replicate). Statistical significance in (**b**–**e**, **g**–**i**) was evaluated using a two-tailed Student's t-test; P-values are indicated. Source data are provided as a Source Data file.

NIL-*HAN2*^{NPB} and *han2* mutants, suggesting that *HAN2* negatively regulates its expression (Supplementary Fig. 14e). This result was consistent with findings from RT-qPCR analysis (Fig. 3e, f and Supplementary Fig. 15a–c). Conversely, no differences in *OsARF24* expression were observed among NIL-*HAN2*^{NPB}, *han2* mutants, and overexpression lines compared with their respective controls (Supplementary Fig. 15d–f). It has been reported that *OsMAP1/OsMPK3* enhanced chilling tolerance in rice by promoting trehalose accumulation[23]. We therefor measured trehalose levels under chilling stress and found that the levels were higher in NIL-*HAN2*^{NPB} than in 93-11 as well as higher in *han2* mutants than in WT (Supplementary Fig. 16a, b). Conversely, trehalose levels were significantly lower in overexpression lines than in WT under chilling stress (Supplementary Fig. 16c). These results indicate that *HAN2* negatively regulates the expression of *OsMAP1/OsMPK3*, which in turn modulates trehalose accumulation and ultimately influences chilling tolerance in rice.

As an auxin transporter, HAN2 may regulate the expression of *OsMAP1/OsMPK3* through auxin signal transduction. ARFs are key components of this signalling and can specifically bind to auxin response elements to activate or repress the transcription of downstream genes[35]. Using a dual-luciferase reporter system in rice protoplasts, OsARF24 was found to inhibit *OsMAP1/OsMPK3* expression (Supplementary Fig. 17). Online predictions using New PLACE revealed an ARF-binding element (TGTCTC) in the upstream region of *OsMAP1/OsMPK3*, which may serve as the binding site for *OsARF24*. Mutation of this element significantly reduced the inhibitory effect of *OsARF24* (Fig. 3g). Subsequent assays, including yeast one-hybrid (Y1H), electrophoretic mobility shift assay (EMSA), and chromatin immunoprecipitation followed by qPCR (ChIP-qPCR), confirmed that *OsARF24* directly binds to the ARF element in the *OsMAP1/OsMPK3* promoter (Fig. 3h–j and Supplementary Fig. 18). Expression of *OsMAP1/OsMPK3* was significantly lower in *OsARF24*-overexpressing lines (*OsARF24*-Flag/ZH11) than in WT (Fig. 3k). To assess the functional relationship between *OsARF24* and *OsMAP1/OsMPK3*, we evaluated chilling tolerance in *osarf24*, *OsARF24*-Flag/ZH11, *osmap1*, and *osmap1/osarf24* plants, with and without exogenous auxin. Compared with their respective WT controls, *OsARF24*-Flag/ZH11, *osmap1*, and *osmap1/osarf24* plants displayed increased sensitivity to chilling stress, whereas *osarf24* mutants exhibited enhanced tolerance in the absence of auxin (Supplementary Fig. 19a–h and Supplementary Fig. 20a–e). Under auxin treatment, *OsARF24*-Flag/ZH11, *osmap1*, and *osmap1/osarf24* plants showed further sensitivity, although the differences in chilling response compared with WT were reduced. These results suggest that *OsARF24* acts upstream of *OsMAP1/OsMPK3*. To explore the relationship between auxin and the *OsARF24* protein, non-denaturing western blot analysis was performed using total protein extracted from mature leaves of *OsARF24*-Flag/ZH11 plants. The results showed that auxin-treated plants had higher levels of free *OsARF24*-Flag protein compared with untreated controls (Fig. 3l), suggesting that elevated auxin levels promote the release of *OsARF24*, thereby enhancing its regulatory effect on target genes. Furthermore, we generated transgenic lines expressing Flag-tagged *OsARF24* in the *han2* mutant background (*OsARF24*-Flag/*han2*). Expression of *OsMAP1/OsMPK3* was significantly lower in *OsARF24*-Flag/*han2* plants than in *han2* controls (Supplementary Fig. 21a). Non-denaturing western blot analysis using protein from mature leaves of *OsARF24*-Flag/ZH11 and *OsARF24*-Flag/*han2* plants revealed that free *OsARF24*-Flag protein levels were higher in *OsARF24*-Flag/*han2* plants (Supplementary Fig. 21b). Collectively, these findings indicate that *HAN2* negatively regulates chilling tolerance in rice potentially through auxin-mediated signalling pathway.

https://doi.org/10.1038/s41467-025-59449-z

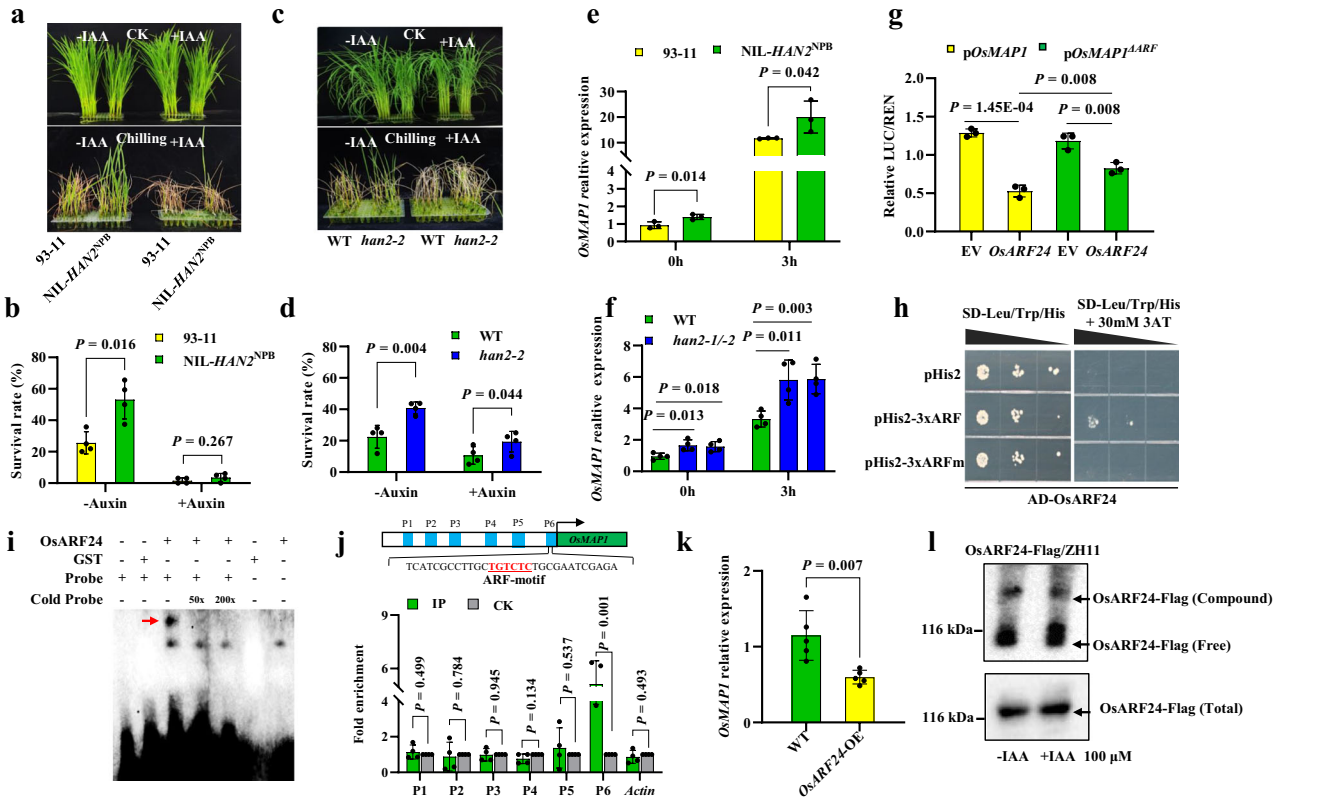

Fig. 3 | Elucidating *HAN2*-mediated chilling tolerance via auxin signalling. **a** Chilling tolerance phenotype of 93-11 and NIL-*HAN2*^{NPB} plants. **b** Survival rates of 93-11 and NIL-*HAN2*^{NPB} plants with and without auxin recovered after chilling treatment. Data are shown as the means ± SD ($n = 4$ biologically replicates, with 16 seedlings per biological replicate). **c** The chilling tolerance phenotype of WT and *han2* plants. **d** Survival rates of WT and *han2* plants with and without auxin recovered after chilling treatment. Data are shown as the means ± SD ($n = 4$ biologically replicates, with 16 seedlings per biological replicate). **e** The *OsMAP1*/*OsMPK3* expression in both 93-11 and NIL-*HAN2*^{NPB} before and after chilling treatment. Data are shown as the means ± SD ($n = 3$ biologically replicates, with 3 seedlings per biological replicate). **f** The *OsMAP1*/*OsMPK3* expression in both WT and *han2* before and after chilling treatment. Data are shown as the means ± SD ($n = 4$ biologically replicates, with 3 seedlings per biological replicate). **g** *OsARF24* negatively regulates the transcriptional activity of *OsMAP1*/*OsMPK3* promoter in rice protoplasts. Data are shown as the means ± SD ($n = 3$ biologically replicates). **h** Y1H assays demonstrate that OsARF24 interacts with ARF-motif elements. **i** EMSA confirms that OsARF24 binds to the ARF-motifs of *OsMAP1*/*OsMPK3* promoter. **j** ChIP-qPCR showing that OsARF24 binds to the *OsMAP1*/*OsMPK3* promoter in vivo. P1-P6, represent DNA fragments from different positions of the *OsMAP1*/*OsMPK3* promoter. Immunoprecipitation was performed with anti-Flag antibody (IP), IgG was used as a negative control (CK). *Actin* used as the internal standard. Data are shown as the means ± SD ($n = 4$ biologically replicates). **k** *OsMAP1*/*OsMPK3* expression in WT and *OsARF24*-OE lines. Data are shown as the means ± SD ($n = 5$ biologically replicates, with 3 seedlings per biological replicate). **l** Distribution of OsARF24 free and compound proteins in *OsARF24*-Flag/ZH11 overexpressing plants with and without auxin. A representative experiment from at least two independent experiments is shown. Significance is evaluated by the two-tailed Student's *t*-test, and *P*-values are indicated. Source data are provided as a Source Data file.

Copia LTR-mediated epigenetic suppression of *HAN2* in *temperate japonica* rice

Within the delimited genomic region, three putative genes were identified (Fig. 1c, Supplementary Fig. 3 and Supplementary Table 1). Among them, *LOC_Os01g50090* encodes a *Copia* LTR located 0.5 kb downstream of the 3′UTR of *HAN2*, which is absent in the *indica* cultivar 93-11. Studies have shown that retrotransposons may influence the expression of the neighbouring gene[36]. To assess its impact on *HAN2* expression, we used CRISPR/Cas9 to delete the retrotransposon in the *temperate japonica* rice cultivar ZH11 (Supplementary Fig. 22a, b). The resulting line, *HAN2*$^{-LTR}$, carried a complete deletion of the retrotransposon (Supplementary Fig. 22c) and exhibited *HAN2* expression level approximately twice those of WT (Fig. 4a). *HAN2*$^{-LTR}$ plants were also more sensitive to chilling stress, displaying a 50.0% lower survival rate compared with WT plants following chilling treatment (Fig. 4b, c). Additionally, we compared promoter polymorphisms of *HAN2* between 93-11 and NPB (Supplementary Fig. 23a). However, no significant difference in *HAN2* promoter activity was observed between the two genotypes in rice protoplasts (Supplementary Fig. 23b). These findings indicate that the significant difference in *HAN2* expression between *indica* and *temperate japonica* rice is attributable to the presence or absence of the *Copia* LTR downstream of *HAN2*, rather than to promoter variation.

To further validate the effect of the *Copia* LTR on *HAN2* function, we compared *HAN2* expression and chilling tolerance across rice varieties with and without the retrotransposon. *HAN2* expression was generally higher in five *indica* rice varieties lacking the LTR than in five *temperate japonica* rice varieties carrying the LTR (Supplementary Fig. 5b), whereas chilling tolerance exhibited the opposite trend (Supplementary Fig. 1a, b). To minimise the influence of ecotype background, we selected two groups of *tropical japonica* rice varieties —those with and without the LTR—for further analysis. *HAN2* expression was significantly higher in *tropical japonica* varieties lacking the retrotransposon, and these varieties exhibited weaker chilling tolerance than those carrying the LTR (Fig. 4d, e). Collectively, these results demonstrate that the *Copia* LTR in *japonica* rice downregulates *HAN2* expression and enhances chilling tolerance.

Insertion of the *Copia* LTR may influence the DNA methylation status of *HAN2*. To test this hypothesis, we analysed *HAN2* methylation levels using a whole-genome DNA methylation database for the *temperate japonica* rice cultivar NPB and the *indica* rice cultivars MH63 and ZS97, both of which lack the

https://doi.org/10.1038/s41467-025-59449-z

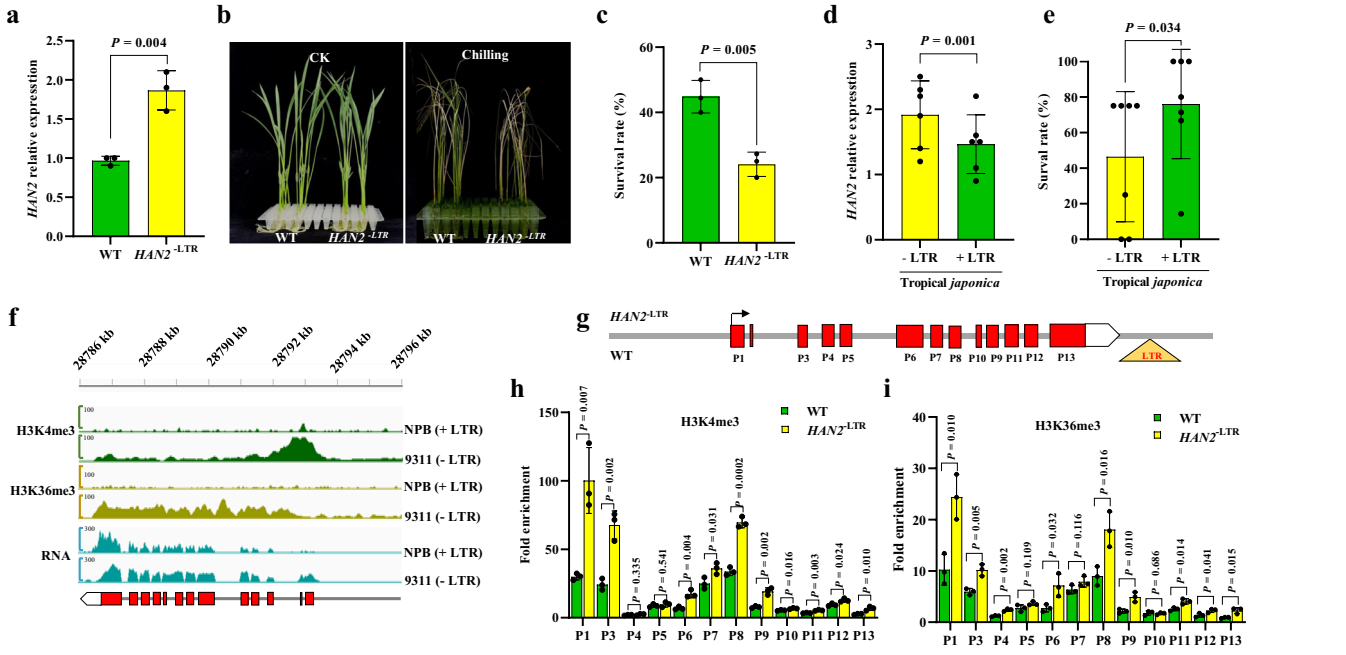

Fig. 4 | CRISPR/Cas9-based dissection of *HAN2*-downstream *Copia* LTR in gene repression. a Expression levels of *HAN2* in WT and *HAN2*^{LTR} plants. Data are shown as mean ± SD ($n = 3$ biological replicates, with 3 seedlings per replicate). **b** Chilling tolerance phenotype of WT and *HAN2*^{LTR} plants. Seedlings were incubated at 4 °C for 5 days and then transferred to normal temperature for a 7 day recovery. Left and right panels show WT and *HAN2*^{LTR} plants before and after chilling treatment, respectively. **c** Survival rates of WT and *HAN2*^{LTR} plants after recovery. Data are shown as mean ± SD ($n = 3$ biological replicates, with 8 seedlings per replicate). **d** Expression levels of *HAN2* in *tropical japonica* rice varieties with or without the *Copia* LTR insertion. Data are shown as mean ± SD ($n = 6$ biological replicates). **e** Survival rates of *tropical japonica* rice with or without the *Copia* LTR insertion after chilling treatment. Data are shown as mean ± SD ($n = 7$ biological replicates). **f** Chromatin modification patterns and transcriptional activity across the *HAN2* gene body. **g** Distribution of ChIP-qPCR fragments within the *HAN2* gene. P1, P2–P13 represent DNA fragments spanning different exons; LTR indicates the *Copia* LTR. **h**, **i** ChIP-qPCR assays showing enrichment of H3K4me3 (**h**) and H3K36me3 (**i**) at the *HAN2* locus in WT and *HAN2*^{LTR} plants. Data are shown as mean ± SD ($n = 3$ biological replicates). Statistical significance in (**a**, **c**–**e**, and **h**, **i**) was evaluated using a two-tailed Student's *t*-test; *P*-values are indicated. Source data are provided as a Source Data file.

retrotransposon (http://glab.hzau.edu.cn/RiceENCODE/). DNA methylation within the gene body of *HAN2* was higher in the two *indica* varieties compared with the *japonica* variety (Supplementary Fig. 24a). To further investigate this, we performed bisulfite sequencing PCR to assess DNA methylation differences in *HAN2* between 93-11 and NIL-*HAN2*^{NPB} and between WT and HAN2-LTR (Supplementary Fig. 24b). In the comparison between 93−11 and NIL-*HAN2*^{NPB}, CG methylation was generally higher in *indica* rice, except at the second position (Supplementary Fig. 24c). However, methylation levels between *HAN2*^{LTR} and WT showed no significant differences, except at the fourth position where WT exhibited higher DNA methylation than *HAN2*^{LTR} (Supplementary Fig. 24d). These findings suggest that DNA methylation within the *HAN2* gene body differs between the *indica* and *temperate japonica* alleles, but this variation is not attributable to the downstream *Copia* LTR insertion.

The *Copia* LTR may influence histone methylation at the *HAN2* locus. To explore this, we analysed the levels of histone modifications H3K4, H3K27, and H3K36 in the gene body region across different *HAN2* genotypes. Active histone marks (H3K4me3 and H3K36me3) were more enriched in the gene body of the *HAN2 indica* allele than in the *temperate japonica* allele (Fig. 4f), whereas the repressive mark H3K27me3 was more enriched in the *temperate japonica* allele (Supplementary Fig. 25a). ChIP-qPCR analysis showed significantly higher enrichment of H3K4me3 and H3K36me3 in the *HAN2*^{LTR} mutant compared with WT, suggesting that the insertion of the *Copia* LTR reduces the enrichment of active histone modifications (Fig. 4g–i). However, H3K27me3 enrichment was also higher in *HAN2*^{LTR} than in WT (Supplementary Fig. 25b), which contrasts with the comparison between 93-11 and NIL-*HAN2*^{NPB}. Collectively, these results indicate that the downstream insertion of the *Copia* LTR in *temperate japonica* rice reduces active histone modifications in the *HAN2* region, thereby suppressing *HAN2* expression.

Copia LTR downstream of *HAN2* enhances rice adaptation to temperate habitats

To examine the distribution of the *Copia* LTR near *HAN2*, we first genotyped a population comprising various rice ecotypes and wild rice accessions using PCR. The *Copia* LTR was present in nearly all *temperate japonica* rice varieties, 50.0% of *tropicaljaponica* varieties, and 27.5% of wild rice accessions but was absent in *indica* rice (Supplementary Fig. 26a). To confirm these observations, we analysed data from the 3000 Rice Genomes Project[37] and obtained consistent results (Fig. 5a and Supplementary Data 1, 2). These findings suggest that the *Copia* LTR adjacent to *HAN2* in *temperate japonica* rice likely originated from wild rice ancestors and that *HAN2* underwent differentiation between *indica* and *japonica* subspecies during domestication.

To determine whether the *Copia* LTR contributed to the adaptation of *japonica* rice to temperate environments, we first analysed fixation indices (F_{ST}), which reflect the level of genetic differentiation between populations. Within a 6.0-Mb region (26–32 Mb) surrounding the *HAN2* locus, a strong differentiation was observed between *indica* and *japonica* rice, with the highest F_{ST} (*Ind*, *Jap*) value reaching 0.71 (Fig. 5b), whereas the genome-wide F_{ST} (*Ind*, *Jap*) value was only 0.55 (Supplementary Fig. 26b). In the region adjacent to *HAN2* (26–32 Mb), the F_{ST} value between *temperate japonica* (*tej*) and *tropical japonica* rice (*trj*) carrying the retrotransposon (*trj*$^{+}$) was low (0.10), whereas the F_{ST} values for *tej* vs. *trj*$^{-}$ (0.78) and *trj*$^{+}$ vs. *trj*$^{-}$ (0.71) were substantially higher (Fig. 5c and Supplementary Fig. 26c, d). These findings indicate

https://doi.org/10.1038/s41467-025-59449-z

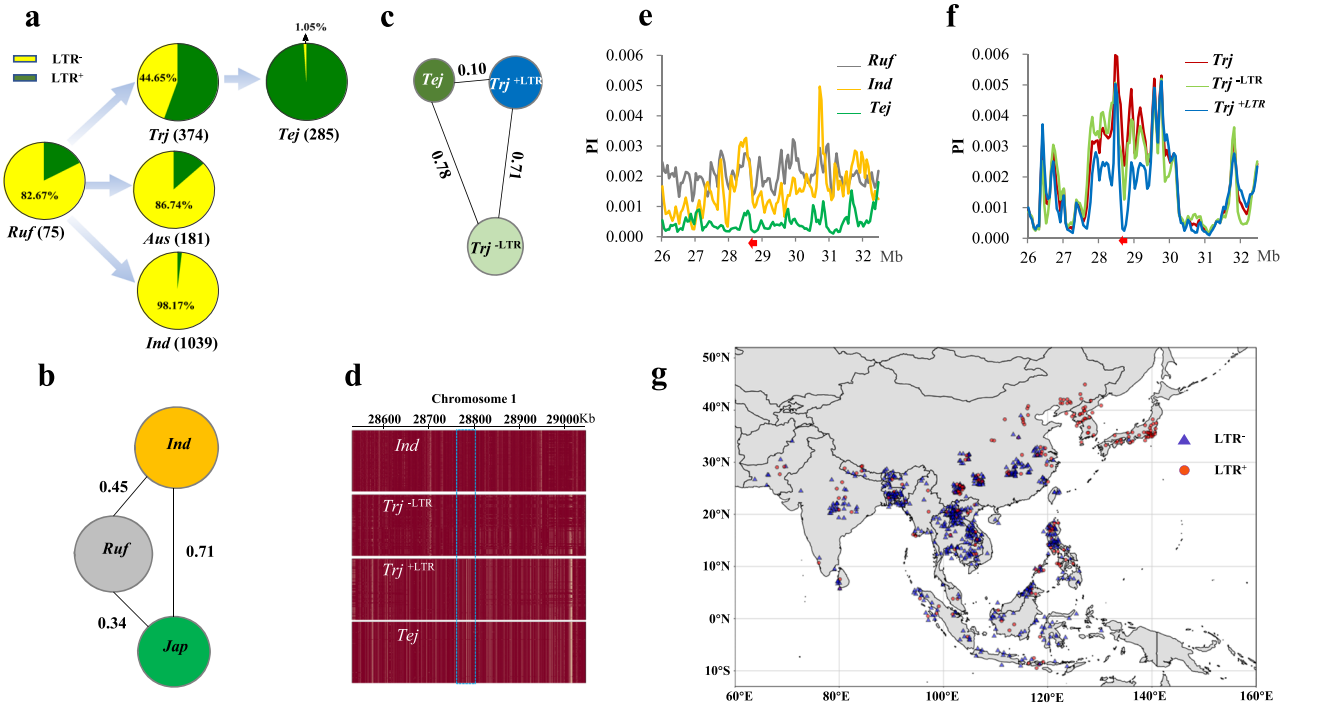

Fig. 5 | Population genetic evidence for adaptive evolution in *HAN2*. **a** Distribution of *HAN2 Copia* LTR across *Aus*, *Ind*, *Trj*, *Tej*, and Ruf populations. **b** Genetic diversity and population differentiation within a 6 Mb region (26–32 Mb) near *HAN2* in *O. rufipogon* and *O. sativa*. Circle sizes represent genetic diversity; F_{ST} values between groups are indicated. *Ruf*, *O. rufipogon*; *Ind*, *indica*; *Jap*, *japonica*. **c** Genetic diversity and population differentiation in a 6 Mb region near *HAN2* in *Tej* and *Trj*. Circle sizes represent genetic diversity; F_{ST} values are indicated. *Tej*, *temperate japonica*; Trj^{-LTR}, *tropical japonica* without *HAN2 Copia* LTR; Trj^{+LTR}, *tropical japonica* with *HAN2 Copia* LTR. **d** Haplotype analysis of the *HAN2* region on chromosome 1 across *indica*, *temperate japonica*, and *tropical japonica* rice with and without the LTR. **e** Nucleotide diversity (π) surrounding the *HAN2* gene in *Ruf*, *Ind*, and *Tej* populations. The red arrow indicates the position of *HAN2*. **f** Nucleotide diversity (π) surrounding the *HAN2* gene in *Trj*, Trj^{-LTR}, and Trj^{+LTR} populations. The red arrow indicates the position of *HAN2*. **g** Percentage and geographical distribution of LTR insertions in rice cultivars across Asian countries. Source data are provided as a Source Data file.

that the retrotransposon may have played a role in the adaptation of *japonica* rice to temperate climates. This inference was further supported by haplotype analysis of a 1.0 Mb region (28.0–29.0 Mb) surrounding *HAN2* using data from the 3000 Rice Genomes Project[37] (Fig. 5d). *Indica* rice lacking the retrotransposon shared a similar haplotype block with *tropical japonica* rice without the retrotransposon, whereas *temperate japonica* rice carrying the retrotransposon exhibited a distinct haplotype block, which was also shared by *tropical japonica* rice with the retrotransposon (Fig. 5d and Supplementary Fig. 26e). Nucleotide diversity analysis revealed that *temperate japonica* rice has lower genetic diversity in the *HAN2* region compared with wild and *indica* rice (Fig. 5e). The Tajima's *D* value for the *HAN2* region in *temperate japonica* rice was −2.65 (Supplementary Fig. 26f), exceeding the 5% significance threshold, indicating a marked reduction in genetic diversity—likely due to positive selection or population migration. Additionally, among *tropical japonica* rice, varieties with the retrotransposon exhibited lower diversity in the *HAN2* region than those without it (Fig. 5f). These results suggest that the genomic region containing the *Copia* LTR downstream of *HAN2* underwent selection during the domestication of *temperate japonica* rice, contributing to its adaptation to temperate environments.

We conducted a geographical distribution analysis of rice varieties across Asia. The results showed that the prevalence of the *Copia* LTR varied by region, ranging from 3.6% in Sri Lanka at low latitudes to 100% in Korea at high latitudes, with intermediate frequencies of 30.4%, 12.6%, and 14.7% in China, India, and Laos, respectively (Fig. 5g). Among the 1039 *indica* rice varieties analysed, only 19 carried the retrotransposon. In contrast, 282 out of 285 *temperate japonica* rice varieties harboured the *Copia* LTR (Fig. 5a). *Indica* rice is predominantly cultivated in low-latitude, low-altitude regions, whereas *temperate japonica* rice is grown in high-latitude, high-altitude environments. These findings suggest that the *Copia* LTR downstream of *HAN2* plays a crucial role in the adaptation of *temperate japonica* rice to colder climates, indicating that *HAN2* was likely subject to selection pressure from chilling stress during domestication.

Suppression of *HAN2* confers dual-stage chilling tolerance and tillering advantage in rice

In addition to the seedling stage, we evaluated the impact of *HAN2* on chilling tolerance during the booting stage. Under normal growth conditions, no significant differences in seed setting rates were observed between 93-11 and NIL-$HAN2^{NPB}$ or between WT and *han2*. However, following chilling treatment at the booting stage, the seed setting rate of NIL-$HAN2^{NPB}$ was significantly higher than that of 93-11, and *han2* mutants exhibited higher seed setting rates than WT (Fig. 6a–f). Given that *HAN2* negatively regulates seedling chilling tolerance in rice, we speculated that *HAN2* may also regulate chilling tolerance during the booting stage via the same mechanism. Then, we measured auxin content in young spikelets of NIL-$HAN2^{NPB}$ and *han2* mutants under chilling treatment. Compared with their respective controls, auxin levels were significantly lower in both NIL-$HAN2^{NPB}$ and *han2* mutants (Fig. 6g, j). RT-qPCR analysis showed that *OsMAP1*/*OsMPK3* expression was higher in young spikelets of NIL-$HAN2^{NPB}$ and *han2* under chilling stress compared with the controls (Fig. 6h, k), whereas *OsARF24* expression did not differ significantly between NIL-$HAN2^{NPB}$, *han2*, and their corresponding controls (Supplementary Fig. 27a, b). Additionally, trehalose content in the young spikelets of NIL-$HAN2^{NPB}$ and *han2* under chilling stress showed a similar trend to that observed during seedling chilling tolerance (Fig. 6i, l). Together, these results indicate that *HAN2* negatively

https://doi.org/10.1038/s41467-025-59449-z

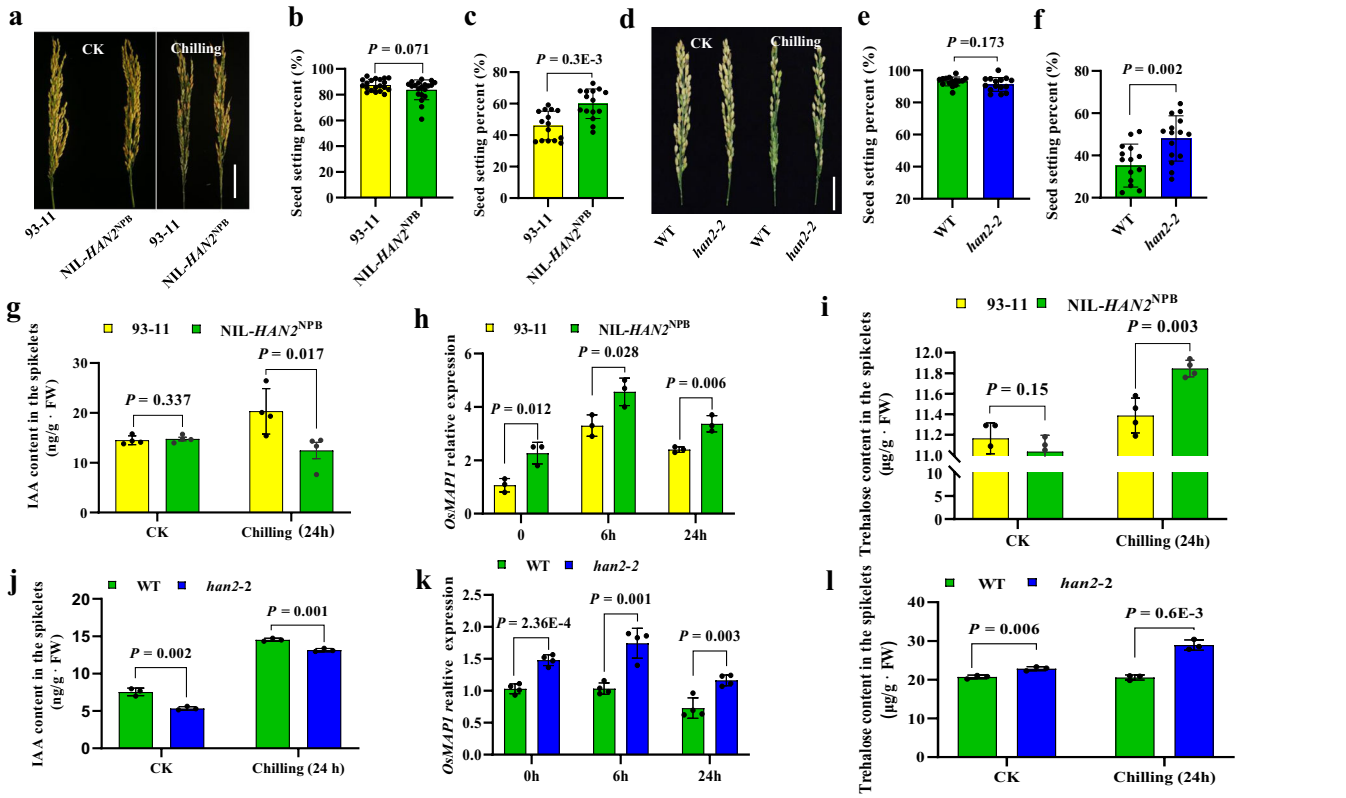

Fig. 6 | Functional analysis of *HAN2* regulation on chilling tolerance at rice booting stage. a Left and right panels show 93-11 and NIL-*HAN2*^{NPB} plants before and after chilling treatment, respectively. Bar = 3 cm. **b** Seed setting rates of 93-11 and NIL-*HAN2*^{NPB} under normal conditions. Data are shown as mean ± SD (n = 20 biological replicates). **c** Seed setting rates of 93-11 and NIL-*HAN2*^{NPB} under chilling conditions. Data are shown as mean ± SD (n = 15 biological replicates). **d** Chilling tolerance phenotype of WT and *han2-2* plants at the booting stage. Left and right panels show WT and *han2-2* plants before and after chilling treatment, respectively. Bar = 3 cm. **e** Seed setting rates of WT and *han2-2* under normal conditions. Data are shown as mean ± SD (n = 15 biological replicates). **f** Seed setting rates of WT and *han2-2* under chilling conditions. Data are shown as mean ± SD (n = 15 biological replicates). **g** Auxin content in spikelets of 93-11 and NIL-*HAN2*^{NPB} after treatment at 19 °C. Data are shown as mean ± SD (n = 4 biological replicates). **h** *OsMAP1*/*OsMPK3* expression in spikelets of 93-11 and NIL-*HAN2*^{NPB} at various time points under 19 °C treatment. Data are shown as mean ± SD (n = 3 biological replicates). **i** Trehalose content in spikelets of 93-11 and NIL-*HAN2*^{NPB} before and after 19 °C treatment. Data are shown as mean ± SD (n = 4 biological replicates). **j** Auxin content in spikelets of WT and *han2-2* before and after 16 °C treatment. Data are shown as mean ± SD (n = 3 biological replicates). **k** *OsMAP1*/*OsMPK3* expression in spikelets of WT and *han2-2* at various time points under 16 °C treatment. Data are shown as mean ± SD (n = 4 biological replicates). **l** Trehalose content in spikelets of WT and *han2-2* before and after 16 °C treatment. Data are shown as mean ± SD (n = 3 biological replicates). Statistical significance in (**b**, **c**, **e**–**l**) was evaluated using a two-tailed Student's t-test; P-values are indicated. Source data are provided as a Source Data file.

regulates chilling tolerance in rice at the booting stage, also potentially through auxin-mediated signalling pathway. Furthermore, transgenic lines overexpressing *HAN2* under the control of either the 35S promoter or the native *HAN2* promoter, as well as CRISPR/Cas9-edited *HAN2*^{LTR} lines, exhibited significantly lower seed setting rates under chilling stress at the booting stage compared with their respective controls (Supplementary Figs. 28a–f and Supplementary Figs. 29a–c). These findings demonstrate that *HAN2* negatively affects chilling tolerance in rice at both the seedling and booting stages.

Auxin plays a key role in regulating plant branching or tillering[38]. We hypothesised that *HAN2* influences rice tillering and, consequently, yield. Field assays conducted in Changsha during the summer of 2023 showed that NIL-*HAN2*^{NPB}, which has reduced *HAN2* expression, produced 1.3 more tillers than 93-11, resulting in a 16.3% increase in yield (Supplementary Fig. 30a–e). Similarly, *han2* mutants produced 3.8 more tillers than WT plants, leading to a 15.2% increase in yield (Supplementary Fig. 30f–j). Field trials conducted in Hainan during the winter of 2023 further confirmed these results: yield per plant in NIL-*HAN2*^{NPB} was 14.7% higher than that in 93-11 (Supplementary Fig. 31a–f), and yield per plant in *han2* was 28.2% higher than that in WT (Supplementary Fig. 32a–f). These findings highlight the potential of the *temperate japonica* rice allele or a loss-of-function *HAN2* allele to not only enhance chilling tolerance at both the seedling and booting stages but also improve rice yield through increased tillering, offering substantial value for breeding programmes aimed at enhancing and stabilising rice production.

Discussion

Rice cultivated in Asia primarily consists of two subspecies: *indica* and *japonica* rice. Typically, *temperate japonica* rice varieties exhibit greater adaptability to chilling stress than *indica* varieties[1,4]. However, the molecular basis underlying this adaptability remains incompletely understood, and the role of auxin in mediating the chilling tolerance of *temperate japonica* rice remains to be fully clarified. Herein, we isolated a chilling tolerance gene, *HAN2*, from *temperate japonica* rice using a map-based cloning approach. *HAN2* encodes an ABCB transporter, OsABCB5, which functions in auxin efflux. The *temperate japonica* allele of *HAN2* contains a downstream retrotransposon insertion that leads to reduced methylation of lysine residues at positions 4 and 36 on histone H3 in the *HAN2* region. This epigenetic modification results in lower transcriptional activity and subsequently alters auxin transport. Compared with the *indica* allele, the *temperate japonica HAN2* allele confers enhanced chilling tolerance at both the seedling and booting stages, largely due to the presence of the retrotransposon insertion (Fig. 7). Our findings further reveal that *HAN2*/*OsABCB5* negatively regulates rice chilling tolerance potentially

through an auxin-cascade involving OsARF24 andOsMAP1/OsMPK3. However, since we don't have direct genetic evidence (i.e. higher order mutants data), we cannot state that *HAN2* could form any signalling module with its potential downstream interactor(s) to mediate chilling adaptation.

Interestingly, *HAN2* regulates auxin levels in plants, similar to other members of the ABCB transporter family, such as *SD8*[39]. However, the mechanism by which *HAN2* influences auxin content remains unclear. The tryptophan-dependent pathway is the primary route for auxin biosynthesis, with YUCCA-encoded flavin monooxygenases catalysing the final rate-limiting step[33]. To explore this further, we analysed the expression patterns of YUCCA family members. Among them, *OsYUC8* exhibited an expression pattern in leaves similar to that of *HAN2* (Supplementary Fig. 12a) and has been reported to influence leaf development (Supplementary Data 3)[40], suggesting that *OsYUC8* is the key target modulated by *HAN2* in leaf tissues. RT-qPCR analysis confirmed that *OsYUC8* expression was significantly lower in NIL-*HAN2*^{NPB} than in 93-11 (Supplementary Fig. 12b), significantly lower in *han2* mutants than in WT plants (Supplementary Fig. 12c), and significantly higher in *HAN2*-overexpressing lines than in WT (Supplementary Fig. 12d). Detached leaf incubation experiments using d_5-Trp further revealed that d_5-IAA synthesis was significantly reduced in *osyuc8* mutants compared with WT (Supplementary Fig. 13b). Moreover, *osyuc8* plants exhibited lower auxin content and a higher survival rate following chilling treatment than WT plants (Supplementary Fig. 13c-e). Based on these results, we propose that *OsYUC8* plays a regulatory role in auxin biosynthesis within mature leaves and that *HAN2* promotes *OsYUC8* expression via an as-yet unidentified feedback mechanism, thereby enhancing localised auxin synthesis.

The d_5-IAA leaf-feeding experiment demonstrated that the relative transfer rate of d_5-IAA was significantly higher in WT plants than in *han2* mutants across multiple leaves (Fig. 2f-g). This finding indicates that *HAN2* facilitates the movement of d_5-IAA from mature source leaves to other plant tissues. Although auxin is primarily synthesised in young tissues, our results show that mature leaves can also produce auxin (Supplementary Fig. 13b). The high expression of *HAN2* in mature leaves likely plays a critical role in transporting auxin synthesised in these tissues to other parts of the plant. This inference is further supported by auxin level measurements in the third to fifth leaves of NIL-*HAN2*^{NPB} and *han2* under both normal and chilling conditions (Supplementary Fig. 33a-d). The main auxin transport proteins located on the plasma membrane include members of the AUX1/LAX, ABCB/PGP, and PIN families, which coordinate the intracellular and extracellular transport of auxin[41]. Auxin uptake is primarily mediated by the efficient IAA^-/H^+ symport mechanism, facilitated by members of the AUX1/Like-AUX1 family[42]. Transcriptomic analysis of NIL-*HAN2*^{NPB} and *han2* revealed no significant differences in the expression levels of *OsAUX* genes across different *HAN2* genotypes, suggesting that *HAN2* does not influence these transporters (Supplementary Fig. 34a-b). Additionally, recent studies have shown that ABCB transporters can promote auxin efflux independently of PIN proteins[43]. However, the efflux of auxin mediated by PINs typically depends on a synergistic mechanism requiring co-localisation with ABCB transporters[43].

The insertion of *Copia* LTR results in reduced enrichment of the active histone marks H3K4me3 and H3K36me3, which collectively downregulate *HAN2* expression and enhance chilling tolerance in both NPB and the *HAN2*^{LTR} mutant (Fig. 4f, Supplementary Fig. 1a-b, and Fig. 4b, c). To date, no studies have specifically reported the effects of *Copia* retrotransposon insertions on histone methylation. However, recent research has shown that a solo-LTR insertion can increase DNA methylation and promote the accumulation of the repressive histone mark H3K9me2, which together suppress *GY3* expression and lead to higher grain yield in the 02428 cultivar and other genetic backgrounds[44]. It is well established that transposable elements can influence the epigenetic regulation of nearby coding genes by promoting the spread of histone methylation marks such as H3K9me2[45]. Therefore, the insertion of the *Copia* LTR downstream of *HAN2* in *temperate japonica* rice may similarly affect histone methylation through a diffusion-like mechanism, thereby modulating *HAN2* expression.

With the intensification of global climate change, achieving high and stable crop yields is essential for ensuring food security. To this end, identifying key genes that contribute to desirable agronomic traits in grain crops is critical. Although numerous genes associated with high yield or abiotic stress tolerance have been identified[46], genes that simultaneously confer high and stable yield remain limited. The *temperate japonica* rice allele *HAN2/OsABCB5* represents a promising example, conferring enhanced chilling tolerance at both the seedling

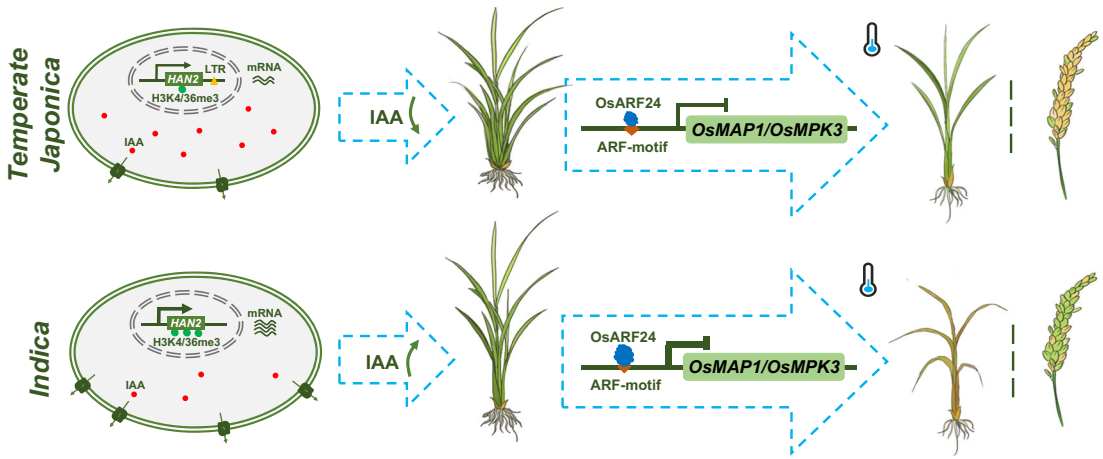

Fig. 7 | Possible working model of *HAN2*-mediated chilling adaptation in rice. *HAN2* encodes the OsABCB5 transporter, which mediates auxin efflux from the cell. In rice, *HAN2* is highly expressed in the parenchyma cells of the vascular bundle sheath in mature leaves, where it facilitates the transport of auxin synthesised in these leaves to young tissues. In *temperate japonica* rice, the insertion of a *Copia* LTR downstream of *HAN2* significantly reduces active histone modifications, including H3K4me3 and H3K36me3, across the gene body, leading to transcriptional suppression of *HAN2*. In contrast, *indica* cultivars lack this retrotransposon insertion, resulting in elevated *HAN2* expression and increased auxin accumulation in young tissues. Higher auxin levels promote the release of OsARF24, which binds to the ARF-motif in the *OsMAP1/OsMPK3* promoter and represses its expression. This regulatory cascade could ultimately compromise chilling tolerance at both the seedling and booting stages in *indica* rice. Conversely, *temperate japonica* rice, which carries the *Copia* LTR insertion, exhibits reduced *HAN2* expression and improved chilling tolerance at both developmental stages.

and booting stages, along with increased tiller number. Following chilling treatment, *OsMAP1*/*OsMPK3* expression in NIL-*HAN2*^{NPB} was consistently higher than that in 93-11 at both stages (Fig. 3e, Supplementary Fig. 15a, and Fig. 6h), and trehalose content was significantly greater in NIL-*HAN2*^{NPB} than in 93-11 (Supplementary Fig. 16a and Fig. 6i). These findings suggest that *HAN2* enhances chilling tolerance across developmental stages, potentially through auxin-mediated signalling pathway. Interestingly, no significant difference in tiller number was observed between *OsARF24* overexpression lines and WT (Supplementary Fig. 35), and yield-related traits such as plant height and effective tiller number remained unchanged in *OsMAP1* knockdown and overexpression lines compared with WT[47]. These results indicate that the regulatory networks by which *HAN2* controls chilling tolerance and tiller number are distinct. The advantageous *HAN2* allele originated from the insertion of an *Copia* LTR downstream of the gene, an element traceable to wild rice. This LTR is present in 5.5% of wild rice, 50.0% of *tropical japonica*, and 97.3% of *temperate japonica* rice varieties (Supplementary Fig. 26a). Among *indica* rice, the insertion is nearly absent, while only 14.3% of the Aus ecotype—believed to have undergone hybridisation with *japonica* rice during domestication[44]—carry the insertion. It is therefore hypothesised that the LTR insertion in *HAN2* originated from wild rice and was selected for in *temperate japonica* rice to support adaptation to cooler climates. Introgression of the *temperate japonica HAN2* allele into *indica* rice improves tillering, grain yield, and chilling tolerance at both the seedling and booting stages, thereby contributing to high and stable yield performance. In *japonica* rice, gene editing techniques can be used to knock out *HAN2*, resulting in improved tillering, yield, and chilling tolerance. Thus, *HAN2* represents a valuable genetic resource for achieving high and stable rice production under climate variability.

Methods

Plant materials and phenotypic evaluations

A set of chromosome segment substitution lines was developed using the *temperate japonica* rice cultivar NPB as the donor and the *indica* cultivar 93-11 as the recipient. From this population, a near-isogenic line, NIL-*HAN2*^{NPB}, was selected and subsequently backcrossed to 93-11 and self-fertilised to generate a fine-mapping population for *HAN2*.

To evaluate chilling tolerance at the seedling stage, 7 day-old seedlings of *indica* or *japonica* rice were exposed to 10 °C or 4 °C in a light incubator for 4–6 days. Following this treatment, seedlings were transferred to a growth chamber set at 28 °C/25 °C with a 13 h/11 h light/dark cycle for a 3–7 day recovery period, after which survival rates were recorded. Plant mortality was defined as the inability to produce new foliage during the recovery phase under ambient conditions after chilling exposure, ultimately resulting in complete desiccation.

To evaluate chilling tolerance at the booting stage, plants at the booting phase—with a distance of −3 to 0 cm between the lamina joints of the flag leaf and the second leaf—were subjected to chilling treatment in a walk-in climate chamber (19 °C for *indica* and 16 °C for *japonica*, 12 h light/12 h dark) for 7 days. Following treatment, the plants were returned to normal growth conditions (28 °C/25 °C, 13 h light/11 h dark) and maintained until full maturity. Seed setting rates were determined using a minimum of four biological replicates per genotype.

Fine mapping of the *HAN2* locus

To fine-map *HAN2*, a genetic segregation population (BC_1F_2) was generated by backcrossing NIL-*HAN2*^{NPB} with 93-11, followed by self-fertilisation. Approximately 3200 individuals from this population were genotyped using seven pairs of molecular markers. By correlating the genotypes of markers M4 and M5 with the chilling tolerance phenotypes of six key recombinant lines (R1–R6), *HAN2* was mapped to a 30.0-kb genomic interval.

Vector construction and genetic transformation

For the genetic complementation of *HAN2*, the *HAN2* coding sequence along with its 2.0 kb native promoter was amplified from the 93-11 genome using primers CP-HAN2-F and CP-HAN2-R. The resulting fragment was inserted into the pCAMBIA1301 vector to generate a fusion construct in which *HAN2* is driven by its native promoter.

To construct an overexpression vector, the full-length *HAN2* gene, including all introns, was amplified from the NPB genome using primers HAN2-OE-F and HAN2-OE-R. The amplified fragment was then cloned into the pCAMBIA1300-EGFP expression vector under the control of the constitutive 35S promoter.

For the *HAN2* knockout, a CRISPR/Cas9-based vector was designed with an sgRNA targeting the exon of *HAN2* under the *OsU6a* promoter.

To knock out the *Copia* LTR, a CRISPR/Cas9-based vector containing two sgRNAs was constructed: one sgRNA targeting the left flanking sequence of the retrotransposon was driven by the *OsU6a* promoter, and the other targeting the right flanking sequence was driven by the *OsU6b* promoter. The complementation vector was introduced into the NIL-*HAN2*^{NPB} line via *Agrobacterium*-mediated transformation, whereas the remaining constructs were transformed into the *temperate japonica* rice cultivar ZH11.

RNA extraction and expression analysis

Total RNA was extracted using the AG RNAex Pro RNA reagent (Accurate, China, AG21102). The extracted RNA was reverse transcribed into cDNA using the HiScript II Q RT SuperMix for qPCR (R223-01, Vazyme). RT-qPCR was then performed using ChamQ Universal SYBR qPCR Master Mix (Q711-02, Vazyme). Gene expression levels were analysed using the ΔΔCt method based on 3–4 biological replicates. Statistical significance was determined using Student's *t*-test.

RNA-seq analysis

Rice shoots were harvested and immediately frozen in liquid nitrogen for RNA-seq analysis. Three biological replicates were included for each sample. RNA sequencing was conducted by BGI using the MGI platform. For data analysis, processed reads were aligned to the reference genome MSURelease7.0[48] using Hisat2 v2.0.1[49]. Gene quantification was performed with HTSeq v0.6.1[50], and differential expression analysis was performed using DESeq2[51]. Differentially expressed genes were identified based on a P-value < 0.05 and an absolute $\log_2$ fold change ($|\log_2 FC| \geq 1$. Gene Ontology enrichment analysis was conducted using the DAVID database (https://david.ncifcrf.gov/home).

Subcellular localisation

The constructed vectors *35S::HAN2-GFP* and *35S::GFP* were introduced into rice protoplasts via PEG-mediated transformation. Following transformation, the protoplasts were stained with 100 μM FM4-64 (a plasma membrane marker) for 1 min, washed with W5 solution, and examined for GFP fluorescence using a confocal laser scanning microscope (LSM880, Carl Zeiss).

DNA methylation analysis

Genomic DNA was extracted from the third leaf of 2 week-old rice seedlings using the SDS method. CpG island regions were predicted and designed using MethPrimer, and bisulfite sequencing PCR (BSP) primers for *HAN2* were designed accordingly (Supplementary Data 4; http://www.urogene.org/cgi-bin/methprimer/methprimer.cgi). The extracted DNA was treated with sodium bisulfite using the EpiTect Bisulfite Conversion Kit (Qiagen). PCR products amplified with BSP primers were ligated into the pEASY Blunt cloning vector (TransGen Biotech), and randomly selected clones were sequenced. CG methylation levels were analysed using Sequencher 5.4.5 software.

ChIP assay

Using ChIP-seq datasets of 93-11 and NPB (SRR10751611, SRR10751742, SRR10751615, SRR10751746, SRR094791, SRR1827950) available in the NCBI public repository[52–54], we analysed histone modifications H3K4me3, H3K27me3, and H3K36me3 in the *HAN2* region.

Leaf samples (4 g) were collected from 2 week-old rice seedlings and cross-linked with 1% formaldehyde. The cross-linking reaction was quenched with 0.125 mol/L glycine. ChIP assays were performed using the EpiQuik Plant ChIP Kit (Epigentek, Brooklyn, NY, USA) with the following antibodies: anti-Flag (#14793, Cell Signalling Technology, Danvers, MA, USA; dilution 1:50), anti-H3K4me3 (A22146, ABclonal, Wuhan, China; dilution 1:50), anti-H3K27me3 (A16199, ABclonal, Wuhan, China; dilution 1:50), and anti-H3K36me3 (A20379, ABclonal, Wuhan, China; dilution 1:50). Chromatin was sheared to fragments of <1000 bp via sonication. Enriched DNA was analysed via RT-qPCR using primers targeting the ARF-motif site in the *OsMAP1*/*OsMPK3* promoter or primers spanning the *HAN2* exon region. ChIP-qPCR assays for H3K4me3, H3K27me3, and H3K36me3 were conducted to compare lines such as WT and *HAN2*^{LTR}. To confirm *OsARF24* binding to the *OsMAP1*/*OsMPK3* promoter, ChIP-qPCR was performed in the *p35S*::*ARF24-Flag* overexpression line. Chromatin precipitated with normal mouse IgG (provided in the kit) was used as a negative control. All primers used are listed in Supplementary Data 4.

Luciferase transient transcriptional activity assay

Using NPB and 93-11 as templates, a 2.0 kb promoter region upstream of the *HAN2* start codon was amplified and cloned into the pGreenII0800-LUC vector to construct the reporter plasmid. The 35S promoter in the pGreenII0800-LUC vector was then replaced with the *HAN2* promoter to generate the *pHAN2*::*LUC* construct. The reporter plasmids were introduced into rice protoplasts and incubated in the dark at 28 °C for 12 h. Protoplasts were then harvested and lysed using the lysis buffer provided in the Dual-Luciferase Reporter Assay Kit (Vazyme, DL101-01). Firefly luciferase activity was measured according to the manufacturer's instructions. *Renilla* luciferase, driven by the 35S promoter in the pGreenII0800-LUC vector, served as an internal control. Relative firefly luciferase activity was calculated as the ratio of firefly luciferase to *Renilla* luciferase activity for each sample.

Determination of auxin content

The method for extracting auxin was carried out according to previously described with minor modifications[55].To analyze the indole-3-acetic acid (IAA) content in 2-week-old rice seedlings under both normal and chilling treatment conditions (4 °C or 10 °C), samples of the shoots or leaves were collected and immediately frozen in liquid nitrogen. 0.1 g sample was weighed into a 1.5 mL tube, mixed with 750 µL cold extraction buffer (methanol: ddH_2O:acetic acid, 80:19:1, v/v/v), vigorously shaken on a shaking bed for 16 h at 4 °C in dark, and then centrifuged at 14,000 × g for 15 min at 4 °C. The supernatant was carefully transferred to a new 1.5 mL tube and the pellet was remixed with 400 µL extraction buffer, shaken for 4 h at 4 °C, and centrifuged. The two supernatants were combined and filtered the mixture into a sample bottle using a nylon filter membrane with a diameter of 13 millimetres and a pore size of 0.22 micrometres (Nylon 66; Tianjin Jinteng Experimental Equipment Co., Ltd.). The samples in the sample bottle will be analyzed for auxin determination using AB SCIEX QTRAP 5500 mass spectrometer.

Determination of trehalose content

The trehalose content was determined according to previously described with minor modifications[23]. Seedlings (0.5 g) were collected at the seedling stage and subjected to low-temperature treatment—either before or after exposure—for 24 h at 4 °C for *japonica* rice or 10 °C for *indica* rice. At the booting stage, young panicles (0.5 g) were collected and treated at 19 °C for 24 h in *indica* rice, either before or after chilling treatment. Samples were ground in liquid nitrogen, and 2 mL of 80% (v/v) ethanol was added. Following centrifugation at 13,000 × *g* for 15 min, the supernatant was collected and heated in boiling water for 20 min and then re-centrifuged at 13,000 × *g* for 10 min. The resulting supernatant was dried at 80 °C, and the residue was dissolved in 4 mL of deionised water and stored at −20 °C until analysis. Before high-performance liquid chromatography, the samples were filtered thrice through a 0.22 µm sterile filter. Each experiment included 3–4 biological replicates, and statistical significance was determined using Student's *t*-test.

Yeast transport experiment

The control vector pYES-MOB-GFP-IST2 and the construct pYES-MOB-*HAN2*-GFP-IST2 were introduced into the yeast strain *INSCV1*. For the d_5-IAA uptake assay, individual yeast colonies were cultured in SD-Ura liquid medium containing 2% glucose at 30 °C with shaking at 200 rpm until the optical density (OD_{600}) reached 0.8. Cells were then harvested through centrifugation at 4 °C and 3500 × *g* for 10 min, washed thrice with sterile water, and resuspended in SD-Ura medium containing 2% lactose, adjusting the OD_{600} to 20. d_5-IAA was then added to a final concentration of 150 µM, and the cell suspension was incubated at 30 °C with shaking at 200 rpm for 3 h. After incubation, cells were washed with 10% methanol followed by sterile water, dried, and subjected to isotope ratio mass spectrometry (MAT253, Thermo Fisher Scientific). Three independent biological replicates were performed for each sample.

In the d_5-IAA efflux assay, yeast clones were cultured in SD-Ura liquid medium containing 2% glucose at 30 °C with shaking at 200 rpm until an OD_{600} of 0.8 was reached. The subsequent steps followed the same protocol as the uptake experiment, except that a portion of the harvested cells was incubated for 12 h in SD-Ura medium containing 2% lactose before further processing. All remaining steps were identical to those used in the uptake assay, including the use of three biological replicates for each sample.

Transport activity assay in *Xenopus* oocytes

Using overlapping PCR, we constructed *pT7*::*GFP* and *pT7*::*GFP-HAN2* expression modules for injection into *Xenopus* oocytes. cRNA was synthesised by in vitro transcription according to the manufacturer's protocol (Yeasen, 10623ES50). A volume of 50 nL of *GFP*, *GFP-HAN2* cRNA, or water (negative control) was injected into selected oocytes using a Nanoject II automatic injector. The oocytes were incubated in modified barth's solution (MBS) at 18 °C for 24 h before transport activity assays. For the uptake experiment, five injected *Xenopus* oocytes were transferred to MBS solution containing 150 µM d_5-IAA and incubated at 18 °C for 4 h. After incubation, oocytes were washed thrice with fresh MBS solution, dried, and prepared for further analysis. Three biological replicates were conducted. For the efflux experiment, injected oocytes were first incubated in MBS solution containing 150 µM d_5-IAA at 18 °C for 12 h. Afterwards, they were washed thrice with fresh MBS solution and transferred to new MBS solution. Five oocytes were collected at 0 and 4 h post-transfer, washed thrice, and dried. Both uptake and efflux samples were analysed using an isotope ratio mass spectrometer (MAT253, Thermo Fisher Scientific).

Protoplast transformation experiment in rice

Protoplasts were isolated from WT and *han2-2* plants[56]. The protoplasts were suspended in pre-cooled W5 solution. For the loading experiment, the protoplasts were centrifuged at 4 °C and 100 × *g* for 10 min. The supernatant was discarded, and the protoplasts were resuspended in pre-cooled W5 solution. Cell concentration was determined using a hemocytometer. Protoplasts were then transferred into 2 mL round-bottom centrifuge tubes, with each tube containing a final d_5-IAA concentration of 75 µM. Twelve tubes were prepared and incubated at 28 °C with gentle shaking at 48 rpm for 0, 0.5, 1, and 2 h. At each time point, three tubes were selected. The protoplasts were

centrifuged at 4 °C and 100 × *g* for 5 min, the supernatant was removed, and the protoplasts were washed 2–3 times with 1 mL of pre-cooled W5 solution and then collected and dried for further analysis.

For the efflux experiment, protoplasts that had been incubated with d_5-IAA for 2 h were washed 2–3 times with pre-cooled W5 solution, resuspended in fresh W5 solution, and transferred to 2 mL round-bottom centrifuge tubes, with 1 mL of protoplast suspension per tube. Twelve tubes were prepared and incubated at 28 °C for 0, 1, 2, and 3 h. At each time point, three tubes were selected. The protoplasts were centrifuged at 4 °C and 100 × *g* for 5 min, and the supernatant was transferred to a new centrifuge tube for further analysis. The protoplasts were then washed 2–3 times with 1 mL of pre-cooled W5 solution, collected, and dried. Both the loading and efflux samples were analysed using an isotope ratio mass spectrometer.

Feeding of d_5-IAA to rice leaves

ZH11 and *han2* seedlings with uniform growth were selected after 3 weeks of cultivation in hydroponic nutrient solution. A 60 μM d_5-IAA solution was applied to the third leaf, positioned approximately 6 cm from the tip, and allowed to absorb for 48 h. After treatment, samples of the treated leaf, leaf sheath, and root tissues were collected, ground into a fine powder, and dried. d_5-IAA levels were measured using isotope ratio mass spectrometry.

GUS histochemical staining and fluorescence immunocytochemistry

The *pHAN2::HAN2-GUS* fusion expression vector, driven by the *HAN2* promoter, was constructed and introduced into NIL-*HAN2*^{NPB} rice via *Agrobacterium*-mediated transformation. Positive transgenic lines were selected for GUS staining and immunofluorescence analysis. GUS histochemical staining was performed on T_3 homozygous transgenic plants. Leaves and leaf sheaths from seedlings were stained, observed, and photographed using a stereomicroscope. For immunofluorescence analysis, the second leaf and second leaf sheath from 3 week-old seedlings were examined using a GUS antibody (Abcam, AB50148; dilution 1:100). Fluorescent signals were visualised with a confocal laser scanning microscope (LSM880, Carl Zeiss).

Identification of the *HAN2*-neighbouring *Copia* LTR

Two pairs of primers were designed to detect the downstream insertion of the *Copia* LTR in 134 rice varieties, including 28 *indica*, 14 *tropical japonica*, 37 *temperate japonica*, and 55 wild rice accessions. The primer pair F/1 R successfully amplified a 368 bp PCR product from NPB genomic DNA, which contains the retrotransposon, whereas no amplification was observed from 93-11 genomic DNA, as the reverse primer (1 R) specifically binds within the retrotransposon, which is absent in 93-11. Conversely, the primer pair F/2 R amplified a 465 bp PCR product from 93-11 genomic DNA lacking the retrotransposon, whereas no amplification was detected from NPB genomic DNA. This is likely because the target region in NPB spans approximately 3.8 kb, exceeding the amplification range of the PCR conditions used.

Y1H assay

The ARF cis-regulatory element from the *OsMAP1/OsMPK3* promoter and its corresponding mutant version (ARFm) were synthesised with three tandem copies and cloned into the pHis2.0 vector via homologous recombination to generate the *pHis2–3 × ARF* and *pHis2–3 × ARFm* constructs, respectively. The full-length coding sequence of *OsARF24* was amplified using PCR from a rice cDNA library and inserted into the pGADT7 vector via homologous recombination to produce the *AD-OsARF24* construct. The Y1H assay was conducted using the Matchmaker Gold Yeast One-Hybrid Library Screening System (Clontech). Briefly, transformants were first plated on SD/-Trp-Leu medium for growth assessment, followed by spotting on SD/-Trp-Leu-His and SD/-Trp-Leu-His media supplemented with 3-amino-1,2,4-triazole for interaction analysis.

EMSA

The coding region of *OsARF24* was amplified from a rice cDNA library and cloned into the pGEX-6P-1 vector via homologous recombination. Protein expression and purification were performed according to the manufacturer's instructions. A biotin-labelled oligonucleotide corresponding to the *OsARF24* binding site was synthesised by annealing equimolar complementary oligonucleotides in Taq DNA polymerase buffer. EMSAs were conducted at room temperature using the EMSA kit (20148, Thermo Fisher Scientific). Briefly, biotin-labelled probes were incubated with either GST or GST-*OsARF24* in binding buffer for 20 min. For competition assays, 50× and 200× molar excesses of unlabelled competitor probes were included. DNA–protein complexes were separated on 5% native polyacrylamide gels, and biotin signals were detected using the ChemiDoc XRS System (Bio-Rad, USA).

Protein extraction and western blot analysis

Total protein was extracted from the shoots or mature leaves of 15 day-old *OsARF24-Flag*/ZH11 and *OsARF24-Flag*/*han2* seedlings using a total protein extraction kit (BestBio, BB-3183) according to the manufacturer's instructions. The extracted proteins were then subjected to non-denaturing western blot analysis. Total OsARF24-Flag protein levels, assessed via SDS-PAGE western blotting, were used as an internal reference. Immunoblot analysis was performed using anti-Flag monoclonal antibodies (CST, D6W5B, dilution 1:1000). All experiments were repeated at least thrice, yielding similar results.

Population genetic analysis of *HAN2*

To obtain the SNPs required for downstream analyses, SNP calling was performed using the VariantFiltration tool in GATK (v4.2.2.0) with default parameters. F_{ST} values were calculated using VCFtools (v0.1.16) with a sliding window of 100 kb and a step size of 50 kb. The map shown in Fig. 6g was generated using the ggmap package in R[57]. Nucleotide diversity within the *HAN2* region across different populations was calculated using DnaSP v5.10[58]. SNPs were imputed using Beagle (v5.1)[59], and haplotype blocks were extracted using plotHaps in vcflib (v1.0.1)[60] and visualised with R (v4.0.2).

Phylogenetic analysis

The full-length protein sequences of ABCB transporters from both rice and *Arabidopsis* genomes were obtained from the Ensembl Plants database (http://plants.ensembl.org/index.html). Sequence alignment was performed using ClustalW in MEGA7[61]. A neighbour-joining phylogenetic tree was then constructed based on the aligned sequences using the Poisson correction method with pairwise deletion of gaps. The reliability of the tree was assessed through bootstrap analysis with 1000 replicates.

Primers

All primers used in this study are shown in the Supplementary Data 4.

Statistical analysis

Statistical analyses were performed using GraphPad Prism 10. Data are presented as the mean ± standard error of the mean. For comparisons between two groups, a two-tailed independent samples *t*-test was used, whereas one-way ANOVA followed by Tukey's multiple comparisons test was applied for comparisons involving three or more groups.

Reporting summary

Further information on research design is available in the Nature Portfolio Reporting Summary linked to this article.

Data availability

Data supporting the findings of this work are available within this paper and its Supplementary Information files. Genetic materials used in this

work are available from the corresponding authors upon request. RNA-Seq and DNA re-sequencing data generated in this study have been deposited in the NCBI/Sequence Read Archive (SRA) database under accession code PRJNA1244014 and PRJNA1244057. ChIP-Seq datasets of 93-11 and NPB are available in the NCBI/Sequence Read Archive (SRA) database under accession code SRR10751611, SRR10751742, SRR10751615, SRR10751746, SRR094791 and SRR1827950. Gene sequence and annotation information is available from the Rice Genome Annotation Project (https://rice.uga.edu/). Source data are provided with this paper.

References

1. Mao, D. et al. Natural variation in the *HAN1* gene confers chilling tolerance in rice and allowed adaptation to a temperate climate. *Proc. Natl Acad. Sci. USA* **116**, 3494–3501 (2019).
2. Li, J. et al. Chilling tolerance in rice: past and present. *J. Plant Physiol.* **268**, 153576 (2022).
3. Lu, G. et al. Rice *LTG1* is involved in adaptive growth and fitness under low ambient temperature. *Plant J.* **78**, 468–480 (2014).
4. Ma, Y. et al. *COLD1* confers chilling tolerance in rice. *Cell* **160**, 1209–1221 (2015).
5. Zhao, J. et al. A novel functional gene associated with cold tolerance at the seedling stage in rice. *Plant Biotechnol. J.* **15**, 1141–1148 (2017).
6. Chen, X. et al. A missense mutation in *Large Grain Size 1* increases grain size and enhances cold tolerance in rice. *J. Exp. Bot.* **70**, 3851–3866 (2019).
7. Liu, H. et al. *OsWRKY115* on *qCT7* links to cold tolerance in rice. *Theor. Appl. Genet.* **135**, 2353–2367 (2022).
8. Li, Z. et al. Natural variation of codon repeats in *COLD11* endows rice with chilling resilience. *Sci. Adv.* **9**, eabq5506 (2023).
9. Xia, C. et al. The COG1-OsSERL2 complex senses cold to trigger signaling network for chilling tolerance in *japonica* rice. *Nat. Commun.* **14**, 3104 (2023).
10. Feng, J. et al. *COG2* negatively regulates chilling tolerance through cell wall components altered in rice. *Theor. Appl. Genet.* **136**, 19 (2023).
11. Liu, D. et al. *COG3* confers the chilling tolerance to mediate OsFtsH2-D1 module in rice. *N. Phytol.* **241**, 2143–2157 (2024).
12. Sun, S. et al. Domestication-selected *COG4-OsbZIP23* module regulates chilling tolerance in rice. *Cell Rep.* **43**, 114965 (2024).
13. Luo, W. et al. COLD6-OSM1 module senses chilling for cold tolerance via 2′,3′-cAMP signaling in rice. *Mol. Cell* **84**, 4224–4238.e9 (2024).
14. Saito, K. et al. Physical mapping and putative candidate gene identification of a quantitative trait locus *Ctb1* for cold tolerance at the booting stage of rice. *Theor. Appl. Genet.* **109**, 515–522 (2004).
15. Zhang, Z. et al. Natural variation in *CTB4a* enhances rice adaptation to cold habitats. *Nat. Commun.* **8**, 14788 (2017).
16. Liu, C. et al. Early selection of *bZIP73* facilitated adaptation of *japonica* rice to cold climates. *Nat. Commun.* **9**, 3302 (2018).
17. Li, J. et al. Natural variation of indels in the *CTB3* promoter confers cold tolerance in *japonica* rice. *Nat. Commun.* **16**, 1613 (2025).
18. Guo, H. et al. Natural variation of *CTB5* confers cold adaptation in plateau *japonica* rice. *Nat. Commun.* **16**, 1032 (2025).
19. Gao, S. et al. CTB6 confers cold tolerance at the booting stage by maintaining tapetum development in rice. *Adv. Sci.* **12**, e2411357 (2025).
20. Fujino, K. et al. Molecular identification of a major quantitative trait locus, *qLTG3-1*, controlling low-temperature germinability in rice. *Proc. Natl. Acad. Sci. USA.* **105**, 12623–12628 (2008).
21. Zhang, C. et al. A transposon insertion in the promoter of *OsUBC12* enhances cold tolerance during *japonica* rice germination. *Nat. Commun.* **15**, 2211 (2024).
22. Zhang, Z. et al. OsMAPK3 phosphorylates OsbHLH002/OsICE1 and inhibits its ubiquitination to activate OsTPP1 and enhances rice chilling tolerance. *Dev. Cell* **43**, 731–743 (2017).
23. Lou, Q. et al. Cold-adaptive evolution at the reproductive stage in Geng/*japonica* subspecies reveals the role of *OsMAPK3* and *OsLEA9*. *Plant J.* **111**, 1032–1051 (2022).
24. Xia, C. et al. Phosphatase OsPP2C27 directly dephosphorylates OsMAPK3 and OsbHLH002 to negatively regulate cold tolerance in rice. *Plant Cell Environ.* **44**, 491–505 (2021).
25. Xie, G. et al. Biochemical identification of the OsMKK6-OsMPK3 signaling pathway for chilling stress tolerance in rice. *Biochem. J.* **443**, 95–102 (2012).
26. Chen, L. et al. OsMADS57 together with OsTB1 coordinates transcription of its target *OsWRKY94* and *D14* to switch its organogenesis to defense for cold adaptation in rice. *N. Phytol.* **218**, 219–231 (2018).
27. Su, C. et al. A novel MYBS3-dependent pathway confers cold tolerance in rice. *Plant Physiol.* **153**, 145–158 (2010).
28. Li, Z. et al. OsGRF6 interacts with SLR1 to regulate *OsGA2ox1* expression for coordinating chilling tolerance and growth in rice. *J. Plant Physiol.* **260**, 153406 (2021).
29. Zhang, M. et al. The *OsWRKY63-OsWRKY76-OsDREB1B* module regulates chilling tolerance in rice. *Plant J.* **112**, 383–398 (2022).
30. Eremina, M. et al. Hormonal control of cold stress responses in plants. *Cell Mol. Life Sci.* **73**, 797–810 (2016).
31. Du, H. et al. A GH3 family member, OsGH3-2, modulates auxin and abscisic acid levels and differentially affects drought and cold tolerance in rice. *J. Exp. Bot.* **63**, 6467–6480 (2012).
32. Lv, Y. et al. New insights into the genetic basis of natural chilling and cold shock tolerance in rice by genome-wide association analysis. *Plant Cell Environ.* **39**, 556–570 (2016).
33. Zhao, Y. Auxin biosynthesis and its role in plant development. *Annu. Rev. Plant Biol.* **61**, 49–64 (2010).
34. Zhao, Y. Essential roles of local auxin biosynthesis in plant development and in adaptation to environmental changes. *Annu. Rev. Plant Biol.* **69**, 417–435 (2018).
35. Li, Y., Han, S. & Qi, Y. Advances in structure and function of auxin response factor in plants. *J. Integr. Plant Biol.* **65**, 617–632 (2023).
36. Cui, X. & Cao, X. Epigenetic regulation and functional exaptation of transposable elements in higher plants. *Curr. Opin. Plant Biol.* **21C**, 83–88 (2014).
37. The 3,000 rice genomes project. The 3,000 rice genomes project. *Gigascience* **3**, 7 (2014).
38. Domagalska, M. & Leyser, O. Signal integration in the control of shoot branching. *Nat. Rev. Mol. Cell Biol.* **12**, 211–221 (2011).
39. Qu, R. et al. Genome-edited ATP BINDING CASSETTE B1 transporter SD8 knockouts show optimized rice architecture without yield penalty. *Plant Commun* **3**, 100347 (2022).
40. Zhou, L. et al. ESCRT-III component OsSNF7.2 modulates leaf rolling by trafficking and endosomal degradation of auxin biosynthetic enzyme OsYUC8 in rice. *J. Integr. Plant Biol.* **65**, 1408–1422 (2023).
41. Zhang, Y., Berman, A. & Shani, E. Plant hormone transport and localization: signaling molecules on the move. *Annu. Rev. Plant Biol.* **22**, 453–479 (2023).
42. Swarup, R. & Bhosale, R. Developmental roles of AUX1/LAX auxin influx carriers in plants. *Front. Plant Sci.* **28**, 1306 (2019).
43. Mellor, N. et al. Systems approaches reveal that ABCB and PIN proteins mediate co-dependent auxin efflux. *Plant Cell* **34**, 2309–2327 (2022).
44. Wu, B. et al. Suppressing a phosphohydrolase of cytokinin nucleotide enhances grain yield in rice. *Nat. Genet.* **55**, 1381–1389 (2023).
45. Eichten, S. et al. Spreading of heterochromatin is limited to specific families of maize retrotransposons. *PLoS Genet* **8**, e1003127 (2012).
46. Wang, L., Guo, Y. & Yang, S. Designed breeding for adaptation of crops to environmental abiotic stresses. *Sci. Sin. Vitae* **51**, 1424–1434 (2021).

47. Li, H. et al. Fine-tuning OsCPK18/OsCPK4 activity via genome editing of phosphorylation motif improves rice yield and immunity. *Plant Biotechnol. J.* **20**, 2258–2271 (2022).
48. Kawahara, Y. et al. Improvement of the *Oryza sativa* Nipponbare reference genome using next generation sequence and optical map data. *Rice* **6**, 4 (2013).
49. Kim, D., Langmead, B. & Salzberg, S. L. HISAT: a fast spliced aligner with low memory requirements. *Nat. Methods* **12**, 357–360 (2015).
50. Simon, A., Theodor, P. P. & Wolfgang, H. HTSeq-a python framework to work with high-throughput sequencing data. *Bioinformatics* **31**, 166–169 (2015).
51. Love, M. I., Huber, W. & Anders, S. Moderated estimation of fold change and dispersion for RNA-seq data with DESeq2. *Genome Biology* **15**, 550 (2014).
52. Zhao, L. et al. Integrative analysis of reference epigenomes in 20 rice varieties. *Nat. Commun.* **11**, 2658 (2020).
53. Zhang, W. et al. High-resolution mapping of open chromatin in the rice genome. *Genome Res.* **22**, 151–162 (2012).
54. Guo, Z. et al. Global epigenomic analysis indicates that epialleles contribute to allele-specific expression via allele-specific histone modifications in hybrid rice. *BMC Genomics* **16**, 232 (2015).
55. Liu, H. et al. A convenient method for simultaneous quantification of multiple phytohormones and metabolites: application in study of rice-bacterium interaction. *Plant Methods* **8**, 2 (2012).
56. Jiang, Y. et al. Isolation and transformation of rice protoplasts. *Bio-Protoc* **101**, e1010125 (2018).
57. Kahle, D. & Wickham, H. ggmap: spatial visualization with ggplot2. *R. J.* **5**, 144–161 (2013).
58. Librado, P. & Rozas, J. DnaSP v5: a software for comprehensive analysis of DNA polymorphism data. *Bioinformatics* **25**, 1451–1452 (2009).
59. Browning, B. L., Zhou, Y. & Browning, S. R. A one-penny imputed genome from next-generation reference panels. *Am. J. Hum. Genet.* **103**, 338–348 (2018).
60. Garrison, E. et al. A spectrum of free software tools for processing the VCF variant call format: vcflib, bio-vcf, cyvcf2, hts-nim and slivar. *PLoS Comput. Biol.* **18**, e1009123 (2022).
61. Kumar, S., Stecher, G. & Tamura, K. MEGA7: molecular evolutionary genetics analysis version 7.0 for bigger datasets. *Mol. Biol. Evol.* **33**, 1870–1874 (2016).

Acknowledgements

We thank Dr. Hongzhao Yuan (Institute of Subtropical Agriculture, Chinese Academy of Sciences) for help with deuterium stable isotope determination assays, Dr. Liwei Xu (Institute of Subtropical Agriculture, Chinese Academy of Sciences) for help with auxin determination assays, Dr. Can Peng(Institute of Subtropical Agriculture, Chinese Academy of Sciences) for help with the subcellular localization assay, Prof. Wallace A. Cowling (The University of Western Australia) for providing valuable comments on the manuscript, Prof. Yonglong Chen and Dr. Guanghui Liu (Southern University of Science and Technology) for help with the *Xenopus* oocytes transport assays, Prof. Kabin Xie (Huazhong Agriculture University) for providing *osmap1* rice mutants. This research was supported by National Natural Science Foundation of China (32071995, Recipient: D. M.), Natural Science Foundation of Hunan Province for Distinguished Young scholars (2021J110041, Recipient: D. M.), The Science and Technology Innovation Program of Hunan Province (2023NK1010, Recipient: W. T.), Hainan Seed Industry Laboratory and China National Seed Group (B23YQ1517, Recipient: D. M.), and Research and Development of Technology for Resource Utilization of Biogas Liquid Based on Integrated Crop-Livestock Systems (NCTIP-XDB18).

Author contributions

D.M. conceived and supervised the project. Y.C., P.L., and D.M. designed the experiments. Y. C. carried out the experiments, including the fine mapping of the *HAN2* locus, collection of chilling-tolerant phenotypes at the booting stage, DNA methylation analysis, yeast transport experiment, protoplast transformation experiment, feeding of d_5-IAA to rice leaves assay. L.H., and Z.L. carried out the experiments, including GUS histochemical staining and fluorescence immunocytochemistry, collection of chilling-tolerant phenotypes in rice seedlings, seedling auxin and trehalose measurements, analysis the expression of *OsMAP1*, *OsARF24*, and *OsYUC8* during the seedling stage, *yuc8* mutant mature leaf d_5-trp incubation experiment and endogenous IAA measurement. P.L., and X.W. carried out the experiments, including luciferase transient transcriptional activity assay, transport activity assay in *Xenopus oocytes*, Y1H assays, EMSA, ChIP-assays. P.L. completed the detection of the distribution of OsARF24 free and compound proteins using denaturing and non-denaturing immunoblotting. B.W., Y.T., and Y.C. completed the population genetic analysis of *HAN2*. Z.H., and Xuan H. completed the molecular marker identification of the *HAN2* population materials and the molecular marker identification of retrotransposons. Xiaojie. H. analyzed the chilling tolerance differences of *HAN2* in different varieties of *indica* and *japonica* rice. Yuqi X. conducted subcellular localization experiments and the genotyping and phenotyping of *osarf24*. W.Z. completed the analysis of methylation and histone methylation modifications. W.T. provided rice germplasm materials and field experiment guidance. Yongzhong X., and C.C. provided theoretical contributions to the project. D.M., Y.C., and P.L. wrote the manuscript. All the authors read and approved the manuscript.

Competing interests

The authors declare no competing interests.

Additional information

Supplementary information The online version contains supplementary material available at https://doi.org/10.1038/s41467-025-59449-z.

Correspondence and requests for materials should be addressed to Donghai Mao.

Peer review information *Nature Communications* thanks the anonymous reviewers for their contribution to the peer review of this work. A peer review file is available.